A new freshwater teleosaurid from the Jurassic of northeastern Thailand

Jérémy Martin, Suravech Suteethorn, Komsorn Lauprasert, Haiyan Tong, Eric Buffetaut, Romain Liard, Céline Salaviale, Uthumporn Deesri, Varavudh Suteethorn, Julien Claude

A new freshwater teleosaurid from the Jurassic of northeastern Thailand

JEREMY E. MARTIN,[1] SURAVECH SUTEETHORN,[2] KOMSORN LAUPRASERT,[2,3] HAIYAN TONG,[2] ERIC BUFFETAUT,[2,4] ROMAIN LIARD,[2] CELINE SALAVIALE,[1] UTHUMPORN DEESRI,[2,3] VARAVUDH SUTEETHORN,[2] and JULIEN CLAUDE[5]

[1]Laboratoire de Géologie de Lyon: Terre, Planète, Environnement, UMR CNRS 5276 (CNRS, ENS, Université Lyon1), Ecole Normale Supérieure de Lyon, 69364 Lyon cedex 07, France, jeremy.martin@ens-lyon.fr;

[2]Palaeontological Research and Education Centre, Mahasarakham University, Maha Sarakham, 44150, Thailand;

[3]Department of Biology, Faculty of Science, Mahasarakham University, Maha Sarakham, 44150, Thailand;

[4]Laboratoire de Géologie de l'Ecole Normale Supérieure, CNRS (UMR 8538), Paris Sciences et Lettres Research University, 24 rue Lhomond, Paris Cedex 05, 75231, France;

[5]Institut des Sciences de l'Evolution, CNRS-UMR 5554, CC 064, Université de Montpellier, 2, Place Eugène Bataillon, 34095 Montpellier, Cedex 5, France

*Corresponding author

ABSTRACT—The core of the fossil record of Teleosauridae, a family of thalattosuchian crocodylomorphs, is well known from western Tethyan marine deposits of the Jurassic. Outside this province, their fossil record is patchy and in need of revision with specimens from Russia, Madagascar and Asia. *Peipehsuchus teleorhinus* is known from the Early or Middle Jurassic of China and teleosaurid specimens were mentioned or preliminarily described from two Jurassic localities in Thailand, yet they were not assigned to a given taxon. Thanks to recent fieldwork, at least 10 individuals represented by cranial material were excavated and prepared from a single Jurassic locality known as Phu Noi in the lower Phu Kradung Formation of northeastern Thailand. Here, we describe these specimens together with disarticulated postcranial elements and erect a new taxon, *Indosinosuchus potamosiamensis* gen. et sp. nov.. Phylogenetic analyses confirm the teleosaurid affinities of the new species, which does not form an exclusive clade with the Chinese teleosaurid *Peipehsuchus teleorhinus*. The presence of teleosaurids at Phu Noi and a preliminary account of its faunal content favor a Middle to Late Jurassic age for the fossil-bearing horizon. In contrast, Cretaceous deposits in Thailand are characterized by goniopholidids and pholidosaurids indicating a faunal turnover in SE Asia across the Jurassic-Cretaceous. As previously shown by isotope data, the new teleosaurid species was a resident of the freshwater environment and co-occurs with remains of exclusively terrestrial taxa such as sauropod, ornithopod and theropod dinosaurs and other freshwater reptiles such as turtles and temnospondyls.

INTRODUCTION

Thalattosuchians were crocodylomorphs of the Jurassic and Cretaceous (e.g., Eudes-Deslongchamps, 1870; Andrews, 1909; Westphal, 1962; Buffetaut, 1982; Mueller-Töwe,

2005, 2006; Gasparini et al., 2000) with a nearly global distribution, being absent only from high latitudes (Martin et al., 2014a). The group is dominated by marine forms with the likely pelagic Metriorhynchoidea showing the most derived adaptations (Hua and de Buffrénil, 1996; Fernández and Gasparini, 2008). Teleosaurids are less derived in their morphology; all are longirostrine, and most probably retained the ability to come onto land (Westphal, 1962). The majority of teleosaurids are recovered from marine habitats, although there are records from freshwater deposits in peninsular Thailand (Buffetaut et al. 1994a) and China (Young, 1948). A freshwater habitus for the teleosaurids of the Late Jurassic Phu Noi locality in northeastern Thailand was recently confirmed using strontium isotope ratios (Martin et al., 2016).

Marine teleosaurids are generally found in marginal/coastal deposits. Fossils from estuarine or brackish environments, for example in the Late Jurassic of Portugal (Krebs, 1967; 1968) or in the Middle Jurassic of Madagascar (Newton, 1893) suggest an ability to shift between habitats, which raises ecological and physiological questions related to salt excretion, migrations, resource use, reproduction or refuge from predators (Martin et al., 2016). The versatile habitat preferences of teleosaurids may have proved selectively advantageous in the context of sea-level and other global environmental changes (Benson and Butler, 2011; Martin et al., 2014a; Tennant et al., 2017), possibly permitting their survival into the Cretaceous, as recently proposed with the report of *Machimosaurus* in the Hauterivian of Tunisia (Fanti et al., 2016).

Most teleosaurid discoveries are from the Jurassic of Western Tethys (e.g. Eudes-Deslongchamps, 1870; Andrews, 1909; Westphal, 1962). Outside this range, the known material is badly in need of revision: from East Asia (Young, 1948; Li, 1993; Buffetaut et al., 1994a), Madagascar (Newton, 1893; Buffetaut et al., 1981) and Central Asia (Efimov, 1988; Efimov and Chkhikvadze, 1987; Storrs and Efimov, 2000). The new report of teleosaurids

from northeastern Thailand thus improves an otherwise poor record outside Western Tethys. Because of their common occurrence in marine deposits, the discovery of teleosaurids in the continental deposits at Phu Noi, Thailand was unexpected. Since the discovery of the Phu Noi fossil site in 2008, a wealth of disarticulated teleosaurid specimens have been unearthed and prepared from this single locality. The deposit shows evidence of aerial exposure with paleosol development and insect burrows (Martin et al., 2016) and in addition to the teleosaurids, contains a known fauna of both aquatic and terrestrial vertebrates. These include hybodont sharks (Cuny et al., 2014), the ginglymodian fish *Isanichthys lertboosi* (Deesri et al., 2014), the xinjianchelyid turtle *Phunoichelys thirakhupti* (Tong et al., 2015) an undescribed freshwater turtle, ornithopods (Buffetaut et al., 2014), theropods (Chanthasit, 2011), and undescribed remains of sauropod dinosaurs, temnospondyls, and pterosaurs (Buffetaut et al., 2015).

Here, we describe in detail the cranial and postcranial anatomy of several teleosaurid individuals recovered at the Phu Noi site. Based on comparisons with other teleosaurids, we propose a new genus and species and test the relationships of the new taxon with a phylogenetic analysis. We also include a preliminary age assessment for the Phu Noi assemblage and discuss evidence accounting for the abundance of disarticulated teleosaurid skeletons in this continental setting.

Institutional Abbreviations

KS, collection numbers for Kalasin Province specimens at Sirindhorn Museum, Sahatsakhan, Thailand; **PRC**, Palaeontological Research and Education Centre, Maha Sarakham University, Thailand. **IVPP**, Institute of Vertebrate Paleontology and Paleoanthropology, Beijing, China.

SYSTEMATIC PALEONTOLOGY

CROCODYLOMORPHA Hay, 1930

THALATTOSUCHIA Fraas, 1901

TELEOSAURIDAE Geoffroy Saint-Hilaire, 1825

INDOSINOSUCHUS POTAMOSIAMENSIS, gen. et sp. nov.

(Figs. 1-13)

Etymology—The genus name refers to the Indochinese tectonic block where the fossils were found. The species name refers to its occurrence in a freshwater habitat (from the Greek *ποταμός*, meaning river) of Siam, the old name of Thailand.

Diagnosis—*Indosinosuchus potamosiamensis* is characterized by the following combination of characters (autapomorphies denoted with*): (1) maxillae touching the posteriorly positioned incisive foramen, which is flanked by a pair of foramina* (Fig. 4C); (2) long and pinched anterior processes of the nasal, reaching the level of the 14^{th}-15^{th} maxillary alveolus; (3) posterior processes of nasals approaching the orbits but not quite preventing prefrontal-frontal contact*; (4) four premaxillary alveoli; (5) 30 maxillary alveoli and (6) 31 dentary alveoli; (7) parietal extending as a long triangle between the supratemporal fenestrae; (8) relatively small rostrum-to-skull length ratio (about 0.66); (9) supratemporal fenestra longer than wide with a width-to-length ratio of about 0.57; (10) small antorbital fenestra. Differs from *Peipehsuchus teleorhinus* in character (4) and IVPP RV 10098 in characters (2), (3), (7), (8); from *Teleosaurus cadomensis* in (5), (6), (9); from *Steneosaurus bollensis*, *Steneosaurus gracilirostris*, *Steneosaurus leedsi*, *Platysuchus multiscrobiculatus*, *Steneosaurus heberti* in (4), (5), (6), (9); from *Steneosaurus larteti* in (3), (9); from *Steneosaurus brevior* in (3), (4), (9); from *Machimosaurus hugii* in (1), (4), (5), (6), (10); from *Lemmysuchus obtusidens* in (1), (10).

Holotype—PRC-11, a complete skull with mandibles.

Referred Material—PRC-239, complete skull with occluding mandible and associated humerus; PRC-238, partial skull with occluding mandible; PRC-240, large fractured skull with associated mandible and a partial femur; PRC-12, complete skull and mandible in a block containing unprepared postcranial elements including a femur, vertebrae and osteoderms; PRC-10, complete skull; PRC-1213, right dentary of juvenile; KS33-209, incomplete skull; PRC-8, right dorsum of the skull with associated osteoderms; PRC-9, a partial skull without the tip of the rostrum; PRC-15, atlas; PRC-16, axis; PRC-17 and 18, two cervical vertebrae; PRC-20 and PRC-21, thoracic vertebra; PRC-19, cervical ribs; PRC-24, a scapula; PRC-26 and 27, two ilia; PRC-27, one ischium; PRC-861, osteoderm; PRC-30, ventral shield.

Locus Typicus—Phu Noi, Phu Phan range, Kham Muang district, Kalasin province, northeastern Thailand.

Stratigraphic Occurrence—Lower part of the Phu Kradung Formation, Khorat Group, Jurassic. For details, see Martin et al. (2016) and discussion below.

DESCRIPTION

General Description and Preservation

When not specified otherwise, the skull and mandible are primarily described from PRC-11 (Figs. 2–6), which represents the best-preserved material of this taxon discovered so far at Phu Noi. Other specimens, such as PRC-12 and PRC-238, provide confirmation of character states, and are referred to explicitly when relevant (Figs. 7–15). As for elements of the braincase and neighboring structural complexes (laterosphenoid, basisphenoid, basioccipital, parietal, squamosal, exoccipital and quadrate) the description mostly relies on

PRC-8. A minimum of 10 individuals are now known from Phu Noi; these include one juvenile and several subadult and adult forms based on size (Table 1).

Fenestrae and Openings

The external nares consist of a single opening, located at the anterior tip of the rostrum (Figs. 2, 3, 5, 6). The nares mostly face anteriorly, with a slight dorsal component. In anterior view, their outline is triangular. Their internal surface faces dorsally and is formed by the premaxillae. The premaxillae meet each other in front of the combined opening where they contribute a dorsally expanded, pointed projection to its anterior rim.

The circular orbits are enclosed posteriorly by the postorbital and jugal. Their orientation has some lateral inclination and is thus not fully dorsal (Figs. 2C, 3C). The entire orbital margin is slightly protruding and delimited by a smooth ridge.

The supratemporal fenestrae are longer than wide (ratio width/length = 0.57), presenting a quadrangular outline (Fig. 1). They are about three times longer than the orbits and occupy most of the dorsum of the skull. The parietal contributes to the medial and posteromedial margin of the fenestrae, the squamosal contributes to the posterolateral margin, the postorbital forms the anterolateral margin, and the frontal forms the anteromedial margin.

The lower temporal fenestrae face laterally and are nearly as long as the supratemporal fenestrae (Figs. 2, 3). They are bounded ventrally by a thin bar of the jugal, dorsally by the postorbital and squamosal, posteriorly by the ascending part of the quadrate, and the quadratojugal forms their posteroventral corner.

The suborbital fenestrae are elongate, approaching but not reaching the level of the anterior orbital margin (Figs. 2, 3, 6). Their shape is complex, with a straight medial margin built by the palatine and a broadly concavo-convex lateral margin. Anteriorly, the suborbital

fenestra is pointed with an anterolateral contribution of the maxilla, whereas posteriorly, it is broadly U-shaped and bordered by the pterygoid and ectopterygoid (posterolaterally).

The choanae are large — as wide as the palatines (Figs. 2, 3, 7). They open through the pterygoid and palatine and their anterior margin lies between the suborbital fenestrae. Their posterior margin is wide, deeply concave and continuous with the ventral surface of the pterygoid plate.

The antorbital fenestra is elongate and oriented obliquely (Figs. 2, 3). It is a slit-like opening, smaller than the orbit, and lies between the lacrimal and maxilla. The lacrimal forms the entirety of its dorsal border, whereas the maxilla forms the ventral border.

The trigeminal foramen opens anteroventrally between the basisphenoid, prootic and laterosphenoid, the latter being marked by a distinct groove on its anterior surface, presumably for conveyance of cranial nerve V (Figs. 3, 10). Although this area is not particularly well preserved, the anteromedial process of the quadrate is free of bony attachment as in other thalattosuchians such as *Pelagosaurus typus*, *Steneosaurus* cf. *gracilirostris*, *Machimosaurus hugii* and metriorhynchids (Holliday and Witmer, 2009; Fernández et al. 2011; Martin and Vincent, 2013; Brusatte et al., 2016). The pterygoid process of the quadrate forms the ventral margin of the foramen ovale but does not contact the posterior descending process of the laterosphenoid, which contributes to the anterodorsal margin of the foramen ovale. The prootic contributes to its dorsal margin (observable in PRC-8). Within the foramen ovale, the basisphenoid is visible in PRC-11 but other bony contribution is difficult to assess because of the crushed condition of the skull.

The orbitotemporal foramen (Figs. 3, 8) opens as a small transverse slit on the posterior region of the supratemporal fossa and is facing slightly dorsally. The parietal and squamosal contribute equally to its dorsal margin. Medioventrally, the foramen is bounded by the prootic, whereas the quadrate contributes most of its ventral margin.

As observed in lateral view (Figs. 3C, 8F), the tympanic opening has no posterior wall, although a limited descending process of the squamosal underlines its posterior limit. Its ventral, anterior and dorsal margins are formed by the quadrate; the dorsal margin consisting of a thin lamina separating the above-lying squamosal (Figs. 6, 8) as in other teleosaurids such as *Teleosaurus cadomensis* (Jouve, 2009) or *Machimosaurus hugii* (Martin and Vincent, 2013). The exoccipital contributes to the inner dorsal wall. The foramen magnum is not well preserved but can be observed in PRC-8 (Fig. 10). It is slightly smaller than the occipital condyle and as is the case in other thalattosuchians, it is bound by the exoccipitals, basioccipital and supraoccipital.

The external mandibular fenestra (Figs. 2C, 3C, 5B) is deep and long, occupying about ten percent total mandibular length. The dentary completes its anterior margin, including the anterodorsal and anteroventral corners. The surangular and angular contribute to its dorsal and ventral margins, respectively. The coronoid is visible through the fenestra.

Skull

Premaxilla—The premaxillae can be observed from different views in PRC-11 (Fig. 4). The dorsal surface is mostly smooth, with ornamentation, including millimeter-sized foramina, more prominent on the lateral and posteromedian dorsal surfaces. A prominent median process is present just anterior to the external nares (Figs. 3, 4, 8). PRC-238 shows only the dorsal and lateral surfaces as the occluding dentary hides its ventral surface. On the ventral surface of PRC-11, the premaxillary-maxillary suture is U-shaped with the convex anterior process of the maxilla extending forward to reach the level of the third premaxillary alveolus. As seen in ventral view, the incisive foramen is close to the premaxilla-maxilla contact and is flanked by a pair of foramina. Medially, near the sutural area, the premaxilla includes a short pillar, which builds the lateral edge of the 3 mm long and slit-like incisive

foramen. Lateral to each pillar, another foramen of similar size is visible (Fig. 4). The incisive foramen is located close to the premaxillary-maxillary suture as in the reconstructions of *Steneosaurus* from Holzmaden (Mueller-Towe, 2005) but unlike *Machimosaurus hugii* (Martin and Vincent, 2013) or *Lemmysuchus obtusidens* (Johnson et al. 2017) whose incisive foramen is completely enclosed by the premaxilla. The condition in PRC-11 is similar to that of the Chinese form IVPP RV 10098, but instead of foramina, a pair of fossae lies lateral to the incisive foramen (Fig. 17).

Posterior to the incisive foramen, the premaxillae do not contact each other medially, due to the anterior projection of the maxillae (Figs. 2, 3, 4). The premaxilla hosts 4 alveoli, which are organized in two pairs (PRC-238 and PRC-11). Their collars protrude anteroventrally for the first two alveoli and lateroventrally for the last alveolus. In the first pair, the first and second alveoli have the same diameter, being slightly smaller than the alveoli of the second pair; i.e., the third and fourth. In each pair, the alveoli are in close contact but not confluent. They are separated by a small diastema accommodating the first dentary tooth. Posterior to the second pair, a long diastema stretches over the premaxilla-maxillary suture. This space accommodates the enlarged double caniniforms of the third and fourth dentary alveoli — a pattern of occlusion particularly well exemplified in PRC-11 (Figs. 2, 3, 4).

Maxilla—The maxillae build a nearly tubular rostrum with straight and parallel lateral edges as is common among teleosaurids. In section, the rostrum is wider than high and presents a convex dorsal margin; the ventral margin is also convex but is depressed along the midline suture. Ornamentation is subtle on the dorsal surface of the maxilla with numerous longitudinal shallow furrows. Elongate foramina are distributed along the lateral surface of the maxilla, just above the tooth row. On the dorsal surface, posteromedial contact between the premaxillae exclude the maxillae from the external nares (Figs. 3, 7, 8). The maxillae

contact each other dorsally for most of the rostrum length but are separated by the nasals at the level of the 15th maxillary alveolus. Posterolaterally, the maxilla contacts the jugal ventrally, the lacrimal dorsally, and contributes to the ventral margin of the antorbital fenestra.

The maxillary alveoli face ventrally with a slight lateral orientation. Medially, a continuous line delimits the alveolar margin from the more ventrally positioned palatal process of the maxilla. A set of anteroposteriorly elongate foramina opens along this line and between each alveolus. In lateral view, alveolar collars are well individualized facilitating a reliable tooth count. In PRC-11, the left maxillary tooth row is not obscured by the occluding mandible and the first 20 alveoli are visible. Sediment hides the remaining length of the tooth row. The CT data reveal a total of 30 maxillary alveoli (Fig. 5). In PRC-238, the left maxillary tooth row is visible in lateral, and to some degree, ventral view, revealing the first 27 alveoli. The posterior part of the tooth row is hidden by the occluding mandible. The occlusion pattern shows that maxillary and dentary teeth are interfingered throughout, leaving no occlusion pits between alveoli 1 and 20. No occlusal pits were detected in the posterior area of the tooth row despite the fact that teeth are not protruding out of the tooth row in this area. The maxillary tooth row ends just anterior to the suborbital fenestra as seen in PRC-11 (Fig. 3) and PRC-240.

In PRC-11, the palate is heavily cracked, but sutures can be identified on the left side (Fig. 2). Here, the maxilla participates in the anterior and anterolateral margins of the suborbital fenestra, where it is strongly convex. In the posterior corner of this convexity, the maxilla contacts the ectopterygoid, preventing a contact with the posterior margin of the tooth row. The maxillary tooth row stops in front of the suborbital fenestra and the ectopterygoid is separated from the posterior border of the tooth row. Laterally, the maxilla shows an extensive contact with the pointed anterior process of the jugal. Medially, the maxilla

extensively contacts the palatine; their contacts ending at the anterior corner of the suborbital fenestra.

Nasal—The nasals are triangular in dorsal view; they are short and extend in front of the antorbital fenestrae but do not extend along the entire length of the rostrum (Figs. 3, 6, 7, 8). Their dorsal surface is smooth, although small foramina are present on their lacrimal margin. Anteriorly, they form a pinched process reaching the level of the 15th maxillary alveolus. Nasal-premaxilla contact is excluded by the elongate maxilla. The dorsal surface of the nasals is inflated just anterior to the orbits and at their medial contact they present a median and elongate depression (Fig. 2). The wide, anterior triangular process of the frontal divides the posteriormost region of the nasals. Here the nasals form a thin process, which curves posterolaterally and approaches but does not reach the orbital margin. Thus, the prefrontal and frontal retain a thin contact along the orbital margin only. Laterally, the nasals extensively contact the medial margin of the prefrontal and more anteriorly they contact the anterior process of the lacrimal.

Postorbital—The postorbital forms the anterolateral margin of the supratemporal fenestra. Its posterior process consists of a thin bar that extends almost two thirds the length of the supratemporal fenestra. Laterally, this process is grooved and bears three foramina (Fig. 2). The postorbital closes the posterior margin of the orbit where it is slightly elevated in a semi-spherical shape. Its dorsal surface is not ornamented. The postorbital bar (Fig. 6A, B) is not inset from the jugal, which leaves the jugal obscured in dorsal view. The postorbital also forms most of the ventral margin of the orbit and sends a massive and short subcircular bar onto the lateral surface of the jugal (Fig. 6A, B).

Jugal—The anterior extension of the jugal is best seen in PRC-11 (Fig. 6A, B). Here it forms the anterolateral margin of the orbit (Figs. 2, 6), contacts the lacrimal along a straight medial suture, and contacts the maxilla laterally. The jugal sends a small, pointed, anterior

process slightly beyond the forward extension of the prefrontal. The jugal is excluded from the antorbital fenestra by the lacrimal (Figs. 3, 6).

The jugal includes a thin but wide plate that bears a broad depression on its ventromedial surface (Fig. 3B) and receives the postorbital bar dorsally. Medioventrally, the jugal accommodates the ectopterygoid. The posterior jugal process extends from the plate and is dorsally concave and flat. It continues for most of the infratemporal length before contacting a short anterior process of the quadratojugal near the posteroventral corner of the infratemporal fenestra.

Frontal—The dorsal surface of the unpaired frontal is flat and ornamented with ovoid to circular pits (Fig. 2). The frontal participates in the posteromedial corner of the orbit and in most of the anterior margin of the supratemporal fenestra, which it overhangs. The anterior process of the frontal is short, but terminates anterior to the orbits, where it divides the posterior tips of the nasals (Figs. 3, 7, 8) and participates in the posterior margin of a slit-like depression. This process reaches the same level as the anterior processes of the prefrontals. The frontal-postorbital suture is V-shaped, pointing in a lateral direction. The frontal contributes to the posteromedian corner of the supratemporal fenestra where it is supported by the laterosphenoid (Figs. 3B, 6A). Posteriorly on the intertemporal bar, the frontal sends a thin and short V-shaped process within the parietal. The frontal forms less than one third the length of the intertemporal bar.

Prefrontal—The tear-drop shaped prefrontal forms the anteromedial margin of the orbit (Figs. 2, 6B, D). Its acute posterior end narrowly contacts the orbital margin of the frontal. As seen in dorsal view, the medial margin of the prefrontal is convex with a broad nasal contact. The prefrontal is longer than wide and its suture with the lacrimal lies near the medial margin of the orbit. The prefrontal sends a short and pointed anterior process between

the lacrimal and nasal. This process runs along a depressed surface, clearly visible on both sides of the skull.

Lacrimal—The lacrimal forms most of the anterior and all of the anterolateral margins of the orbital rim (Figs. 2, 6B, D). It is about two times longer than the medially bordering prefrontal and contacts the nasal along its anteromedial border (Fig. 2). The lacrimal-jugal suture is difficult to follow but the jugal prevents a lacrimal-postorbital contact along the orbital margin. The lacrimal forms the dorsal and posterior margin of the antorbital fenestra. The bone projects slightly anterior to this fenestra. The anterior tip of the lacrimal is pointed.

Parietal—The parietal forms most of the intertemporal bar (Figs. 3, 6A). Its dorsal surface is narrow anteriorly but expands posteriorly to give the dorsum of the skull a triangular shape. Here, the parietal is ornamented with a few oval and well-spaced pits. The parietal reaches the occipital margin where it covers the supraoccipital. Lateral to the intertemporal bar, the parietal is almost vertical. Much of the posterolateral parietal process forms the posterior wall of the supratemporal fossa and faces anterodorsally. Together with the squamosal, the parietal participates in the dorsal portion of the mediolaterally elongated orbitotemporal foramen (Figs. 2, 3, 10). Within the supratemporal fossa, the parietal forms extensive sutures with the laterosphenoid and prootic.

Supraoccipital—The supraoccipital is covered dorsally but visible posteriorly between the parietal and exoccipital. The post-temporal foramen is large (Fig. 10H) and pierces the supraoccipital dorsolaterally. Its roof is formed by the parietal.

Squamosal—The squamosal forms the posterolateral portion of the supratemporal fossa and sends an elongate process along the lateral margin of the supratemporal fenestra. Its anterior process nearly reaches the anterior half of the fenestra where it is overlapped dorsally by the posterior process of the postorbital to complete the supratemporal arcade. The large

posterior squamosal surface is smooth, faces anterodorsally and slopes within the supratemporal fossa. The squamosal forms the laterodorsal margin of the orbitotemporal foramen. Along the posterior margin of the skull roof, PRC-8 is sufficiently well preserved to show two outgrowths for muscle or tendon attachment (Fig. 10), possibly for M. depressor mandibulae. The posterolateral portion of the squamosal projects ventrally and forms the dorsal wall of the otic recess. Dorsally, the squamosal houses a shallow and slightly concave surface (Fig. 6C) common in thalattosuchians (e.g., Martin and Vincent, 2013).

Exoccipital—The exoccipital is a complex structure. Its dorsal margin is medially high but rapidly descends laterally. The exoccipital bears a prominent lateral process visible in dorsal view and clearly projecting from the occipital margin. Anterolateral to the process, the exoccipital contacts the ventral process of the squamosal described above. Ventrally, the exoccipital overhangs the exoccipital plate, which is well developed laterally and sits on the medial quadrate condyle. Those two exoccipital plates enclose the large and deep cranioquadrate passage (Figs. 6C, 10H, F). The lateral-most wall of this passage is formed by the exoccipital, which is notched at this level and connects to the otic area. Here, the squamosal and quadrate do not meet and do not prevent the cranioquadrate passage from entering the otic area. The medial area of the exoccipital bears a circular foramen for cranial nerve XII, which sits above the level of the occipital condyle. The foramen vagi opens laterally, at the same level as the occipital condyle (Fig. 10).

Basioccipital—The basioccipital forms the occipital condyle and a ventrally short but complex basioccipital plate (Fig. 10). The right basioccipital tuberosity is preserved, indicating the process is bifurcated as in other teleosaurids. Laterally, the basioccipital tuberosity displays a prominent process just ventral to the exoccipital suture. Here, the foramen for the carotid artery is located on the lateral margin of the tuber at the limit between the basioccipital and the exoccipital. This foramen is much smaller than in other

thalattosuchians — a condition previously discussed in relation to salt water tolerance (Herrera et al. 2013; Wilberg 2015a). A large ovoid fossa corresponding to the eroded lateral Eustachian opening is visible at the base of the basioccipital in PRC-8 and PRC-9.

Basisphenoid—As seen in ventral view (Figs. 2, 7), the basisphenoid occupies a large surface anterior to the basioccipital and posterior to the pterygoid. Its anterior margin sends a triangular process into the palatal portion of the pterygoid. The basisphenoid is laterally bounded by the quadrate. The basisphenoid is longer than wide and presents on its ventral surface a pair of V-shaped ridges (Fig. 9). The median Eustachian foramen is delimited anteriorly by the basisphenoid. This foramen is clearly visible between the basioccipital tuberosities.

Quadrate—The quadrate ramus is short and mediolaterally expanded so that it is not visible in dorsal view. The quadrate ramus does not project posteriorly beyond the level of the occiput. The condylar surfaces face posterolaterally. The medial hemicondyle is concave and is taller than the lateral hemicondyle, which is convex. Dorsally, the medial hemicondyle is barely exposed due to the lateral extension of the exoccipital. The dorsal ramus of the quadrate penetrates the supratemporal fossa, forming the ventral margin of the orbitotemporal foramen (Fig. 10B). Dorsolaterally, the quadrate sends an anterior process below the squamosal along the first third of the supratemporal margin. Behind this process, the quadrate forms the anterior and ventral margin of the otic area, as well as the anterodorsal margin via a thin lamina (Fig. 6C). The ventral surface of the quadrate bears a broad but faint muscle scar spanning most of the mediolateral length of the bone. Medially, the quadrate surrounds the ventral margin of the foramen ovale. The primary head of the quadrate sutures with the squamosal and the prootic but does not reach the laterosphenoid. Ventral to the foramen ovale, the pterygoid process of the quadrate does not contact the laterosphenoid, as they are separated by the trigeminal canal of the foramen ovale (Fig. 6A). In PRC-11, the dorsal

surface of the quadrate ramus bears a wide and shallow ovoid depression (Fig. 6C), as in *Machimosaurus hugii* (Martin and Vincent, 2013).

Quadratojugal—The quadratojugal can be seen on the right side of PRC-11, where it forms the posteroventral corner of the lower temporal fenestra, excluding the jugal from this area. It extends slightly anteriorly along the infratemporal bar (Fig. 3). The quadratojugal is smooth and does not seem to ascend along the dorsal margin of the fenestra. In lateral view, it hides the lateral hemicondyle of the quadrate. There is no quadratojugal spine.

Pterygoid—The pterygoid forms the posterior area of the suspensorium. In ventral view (Figs. 2, 8), the pterygoid wings are poorly developed, allowing observation of the ventral surface of the quadrate. The medial body of the pterygoid consists of a thin lamina, which builds most of the roof of the choanae. In ventral view, the choanae are elongate and occupy most of the ventral surface of the pterygoid, opening posteriorly in the continuity of the basisphenoid. The choanae are shallow in their pterygoidal portion and are divided by a well-marked septum that runs along the entire pterygoid length into the palatine. The palatine-pterygoid suture sits anterior to the posterior level of the suborbital fenestra. The pterygoid participates in the posterior margin of the suborbital fenestra where it contacts the ectopterygoid laterally. The posteromedial edge of the pterygoid accommodates the pointed anterior process of the basisphenoid. The bony *torus transiliens* is positioned anterior to the posteromedial margin of the pterygoid (Fig. 8). It is dorsally inflated and has the shape of a pea in lateral view.

Ectopterygoid—The ectopterygoid participates in the posterior half of the lateral margin of the suborbital fenestra and extends within the posterior level of the orbits (Figs. 3, 10). The bone is flat and sutures with the ventral margin of the pterygoid wing. The ectopterygoid does not reach the posterior-most level of the pterygoid *torus transiliens*. Anteriorly, the ectopterygoid contacts the palatal process of the maxilla. The ectopterygoid is

separated from the tooth row by a long posterior palatal extension of the maxilla (Figs. 2, 7). The ectopterygoid contacts the jugal anterodorsally.

Palatine—The anterior portion of the palatine is best preserved in PRC-11 whereas the posterior portion is best preserved in PRC-238. The anterior process of the palatine consists of a long and thin triangular projection between the maxillae, reaching the level of the 18th maxillary alveolus in PRC-11, where the rostrum becomes constricted (Fig. 2). At the level of the 21st or 22nd maxillary alveoli, a pair of small and longer-than-wide foramina pierces the ventral surface of the palatines near the anterior suture with the maxilla (Figs. 3B, 7D). In the continuity with these foramina, a pair of shallow grooves extends onto the ventral surface of the maxilla. The palatine contributes to the entire medial surface of the suborbital fenestra. In this area, and posteriorly until the level of the choanae, the lateral edges of the palatine remain parallel to each other. The palatine-pterygoid suture is difficult to discern in most specimens. On the left side of PRC-11, the palatine contributes to the lateral wall of the choanae, thus the pterygoid may be participating in the posteromedial corner of the suborbital fenestra. The choanae occupy most of the palatal width. A prominent pterygoid septum divides the anterior area of the choanae and seems to connect both dorsal and ventral margins of the palatine. The lateral margin of the palatine is almost parallel to the medial margin of the ectopterygoid. The palatine is wide — even wider than one suborbital fenestra. In PRC-238, the incomplete nature of the skull roof allows the palatine to be observed in dorsal view. It bears numerous cracks and is slightly inflated dorsally.

Laterosphenoid—The laterosphenoid is well preserved in PRC-11 and in PRC-8 (Figs. 3, 6, 10). Its main body is anteroposteriorly elongate and has a solid dorsal connection with the frontal and parietal along the medial wall of the supratemporal fossa. The laterosphenoid capitate process is spatulate and seems to contact the postorbital only with its anterolateral-most tip. The laterosphenoid contributes to the anterodorsal margin of the

trigeminal foramen (Figs. 6, 10) where it shows a distinct groove for cranial nerve V. Dorsal to this groove, the laterosphenoid contacts the prootic. This sutural area is slightly inflated and delimiting insertions for Mm. pseudotemporalis superficialis and adductor mandibulae externus profundus (Fig. 6A) as described by Holliday and Witmer (2009). Running anteroventrally from the trigeminal opening, a marked groove corresponds to the ophthalmic branch of the trigeminal nerve. However, it is uncertain whether this groove runs on the laterosphenoid or on a dorsal portion of the pterygoid. Assuming this groove is formed by the pterygoid, there would be no contact between the laterosphenoid and quadrate.

Prootic—The prootic is not discernible from other bones of the braincase in most specimens but can be detected in PRC-11 where it is cracked, as well as in PRC-8 where its sutures with other bones of the posteromedial region of the supratemporal fossa are visible (Figs. 3, 6, 10). In its lateral-most region, the prootic is thin and forms the ventral margin of the orbitotemporal foramen. More medially, the prootic expands dorsoventrally and dorsally, it possesses an extensive contact with the parietal dorsally and abuts the laterosphenoid anteriorly, above the level of the opening for the trigeminal nerve.

Endocast—A rubber cast from the endocranial cavity of PRC-8 allows some features to be described from the right side of the endocast (Fig. 10). The cerebrum is clearly visible with its lateral bulbous expansion typical of thalattosuchians (Brusatte et al. 2016; Pierce et al. 2017). The constriction separating the cerebrum from the cerebellum appears narrower than in *Steneosaurus* sp. (Brusatte et al. 2016) or in *Pelagosaurus typus* (Pierce et al. 2017). The olfactory tract is long and its dorsal surface is straight. The specimen does not preserve the olfactory bulbs and it is unknown whether the tract is bifid as in *Pelagosaurus typus* (Pierce et al. 2017). Ventral to the cerebrum, there is a small expansion that topologically corresponds to the pituitary gland (pituitary fossa) of other crocodylomorphs. However, its small size may indicate poor preservation. Ventral to the cerebellum, the branch for the trigeminal nerve is

visible and is directed anteroventrally. Lateral to the cerebellum, an extensive concave surface accommodates the tympanic bulla. Dorsal to it, a poorly preserved crest might indicate the position of the dorsal branch of the longitudinal sinus. Posteriorly, the medulla oblonga is preserved.

Mandible

The mandibular elements are available in six specimens, the best example being PRC-11. Ornamentation occurs only on the lateral and ventral surfaces of the dentary, with small circular foramina in the anterior area (Figs. 2, 3). From the middle of the dentary, the foramina are elongate and aligned craniocaudally. At the level of alveolus 26, there is an elongate groove (nearly 3 cm long in PRC-11).

Dentary—The dentary symphysis is extensive, incorporating the first 16 alveoli (Figs. 2, 3). Its anterior-most area is forked. The morphology of the dentary mirrors that of the maxilla with a convex occlusal surface and alveoli facing slightly dorsolaterally. The dentary tooth rows remain straight and parallel for most of their length; i.e., corresponding to the entire length of the mandibular symphysis, except for the last five alveoli, where the tooth row turns gently outward. The alveoli progressively decrease in diameter toward the posterior end of the tooth row. In lateral view, the tooth row is straight, except at the level of the enlarged third and fourth alveoli (Figs. 2, 3). A set of small foramina borders the medial side of the alveoli along a ridge running for the entire length of the dentary. As seen in lateral view, the dentary forms the anterior margin and sends a process along the dorsal and ventral margins of the external mandibular fenestra.

The first dentary alveolus is large and protrudes anteriorly. A smaller and more laterally protruding alveolus follows. A pair of confluent alveoli comprises the large alveoli 3 and 4, which are distinctly raised above the remaining dentary tooth row and occlude in the

diastema located on the posterior edge of the premaxilla. Ventrolateral to the pair, the dentary alveolus 5 opens more laterally than any other alveoli in the tooth row, giving the mandible a distinct profile (also seen in PRC-238) — condition is found in other teleosaurids. The right dentary alveolar count of PRC-11, the most complete specimen, is 31 and this is confirmed by the CT data (Fig. 5). This count is in the range of some teleosaurids such as *Lemmysuchus obtusidens* or *Steneosaurus durobrivensis* (Andrews, 1913; Johnson et al. 2017) but unlike that of *Machimosaurus* (19 to 22 alveoli; Martin and Vincent, 2013) or the longirostrine *Steneosaurus leedsi* (43 to 44 alveoli; Andrews, 1913).

Splenial—The ventral surface of the splenial shows fine striae (Figs. 2, 9), except near the posterior margin of the symphysis where some shallow furrows are present. The splenial strongly contributes to the mandibular symphysis, reaching anteriorly onto the dorsal surface at the level of dentary alveoli 16-17 and extending posteriorly to the level of the 25th dentary alveolus. In ventral view, the pointed tip of the splenial reaches further anteriorly, toward dentary alveoli 13 (Figs. 2, 3, 9). The symphysis reaches the level of the 20th alveolus in *Machimosaurus* (Martin and Vincent, 2013), the 24th alveolus in *Lemmysuchus obtusidens* (Andrews, 1913; Johnson et al. 2017) and the 33rd alveolus in the longirostrine species *Steneosaurus leedsi* (Andrews, 1913). Posteriorly, the splenial forms the medial margin of the mandibular ramus, extensively meeting the angular. Posterior to the mandibular symphysis, the splenial remains thick medial to the posterior dentary tooth row. The splenial projects posteriorly further and contacts the anterior surangular process. As observed in medial view, the splenial sends a posterior rod-like process along the ventral margin of the medial mandibular fossa, which contacts the anterior process of the prearticular.

Coronoid—The coronoid is not clearly identified but seems to correspond to a wide lamina forming the anterior margin of the medial mandibular fossa, as seen on the right side of PRC-11 (Figs. 2A, 3A). The coronoid seems to be bounded anteriorly and ventrally by the

splenial and may contact the dentary laterally. As observed in occlusal view, a long bony groove is pinched between the splenial and dentary and stretches from dentary alveolus 23 until the anterior tip of the surangular (Fig. 3A). A similar structure was attributed to the coronoid in *Steneosaurus leedsi* by Andrew (1913) and *Lemmysuchus obtusidens* by Johnson et al. (2017).

Angular—The angular contributes to the ventral and posteroventral margin of the external mandibular fenestra (Figs. 2, 3). As observed in lateral view, the angular reaches two-thirds of the mandibular height posterioly. The angular posteroventral margin is gently curved with a convex shape. The angular reaches the posterior-most tip of the retroarticular process, wrapping around the ventral margin of the articular. The surangular-angular suture is nearly straight on the lateral surface of the mandible and intersects the posterior margin of the external mandibular fenestra at mid-height. Within the external mandibular fenestra, the medial surface of the angular is slightly concave and smooth. Medially, the angular is flat and exhibits a long groove, which stretches to the posterior-most tip of the mandible. As observed in medial view, this flat surface of the angular provides a distinct rim on the posteroventral margin of the mandible. As seen in medial view, the angular accommodates a splenial-prearticular contact. Here, the angular is not inflated and the muscular anchor that receives the attachment of the medial mandibular musculature is not developed. As observed in ventral view, in its anterior area, the surface of the angular is flat and wide. It also sends a long anterior pointed process that wedges between the splenial medially, and the dentary laterally. In its posterior region, the ventral surface of the angular consists of a thin ridge, which does not show any lateral or medial extension for adductor musculature attachment.

Surangular—The surangular extends from the level of the orbit almost to the tip of the retroarticular process (Figs. 2, 3). As in most teleosaurids, the surangular consists of a thin bar that contributes to the dorsal and posterodorsal margin of the external mandibular

fenestra. In lateral view, the surangular sends a thin and elongate posterior process that becomes pinched between the angular and articular. This process nearly reaches the posterior-most tip of the retroarticular process. At the level of the articular glenoid fossa, the surangular expands dorsally and hides the articular in lateral view. There, on the lateral surface of this expansion, a small half-moon shaped pit is visible. In the area anterior to the external mandibular fenestra, the surangular sutures over the dentary. Medially, the anterior-most process of the surangular contacts the splenial. The surangular approaches the posterior-most dentary alveolus but does not send any process lateral or medial to the dentary tooth row. The dorsal surface of the surangular remains thin and smooth throughout the length of the bone.

Prearticular—The medial surface of the articular is visible on the right mandibular ramus of PRC-11 but is highly fractured. Here, a prearticular is likely present, covering the medial surface of the articular foot. The prearticular sends an anterior laminar process over the angular, along the ventral margin of the medial mandibular fossa. Anteriorly, this process seems to contact a posteriorly elongated projection of the splenial, as clearly seen on the left element of PRC-238 (Fig. 8). Although this bone is difficult to examine due to its internal anatomical position, the presence of a prearticular may be a symplesiomorphy of Thalattosuchia because it is shared by metriorhynchoids (Andrews, 1913) and by teleosaurids (Martin et al. 2015).

Articular—The articular has a long triangular outline in dorsal view (Figs. 2, 3). It includes a posterodorsally oriented prominent retroarticular process bearing a well-developed mediodorsal projection. This projection is in line with the posterior transverse buttress of the glenoid that separates the glenoid fossa from the retroarticular process. On its dorsal surface, the retroarticular process is demarcated by an acute ridge running anteroposteriorly, which separates a medial fossa from a lateral one. The posterior tip of the retroarticular process is rounded. The transverse buttress of the glenoid is wavy, matching the posterior margin of the

quadrate. The lateral glenoid fossa is twice as wide as the medial glenoid fossa and both areas are delimited by an oblique curve that fits into the quadrate condylar ridge. The foramen aëreum cannot be identified with certainty. On the medial side, the articular surface is deeply concave and hosts a foramen in its inner-most corner. In lateral view, the retroarticular process is posterodorsally curved and does not surpass the articular glenoid cavity (Figs. 2, 3).

Dentition

All teeth have a slender conical shape. Their apex is pointed and the crown is curved. Although the enamel thickness is variable and depends on various parameters including tooth position or tooth size along the tooth row; as an indication, the enamel has a thickness of 50 µm near the apex of a sectioned tooth with a total diameter of 0.2 cm (Fig. 11). Mesiodistal carinae are present but can be mistaken with the numerous, small, and similar-sized apicobasal ridges ornamenting the labial and lingual surfaces of the enamel. Positive identification of the mesiodistal carinae is established on the cross section of a tooth, where both the external surface of the enamel and the underlying enamel-dentine junction show the position of carinae (Fig. 11C). According to such a view in cross section, ridges ornamenting the external surface of the enamel show no corresponding patterns at their underlying level (i.e., below at the enamel-dentine junction). On their external surface, the mesiodistal carinae are smooth and devoid of pseudo-denticles.

Axial Skeleton

All vertebrae are amphicoelous. As indicated by the nearly complete and fully articulated vertebral column (PRC-22, Fig. 12), the axis connects with a suite of 7 cervicals, 15 thoracals (dorsals), 2 sacrals and the first 2 caudal vertebrae. No notable anatomical differences were detected with other teleosaurids.

Atlas-Axis— Specimen PRC-15 (Fig. 12A, B) preserves the intercentrum and the fragmentary right neural arch connected to it. In ventral view, this specimen shows a small ventral process. Posterior to it, the median excavation is wide and shallow and separates a pair of knobs for the articulation of the atlantal ribs. In another specimen, PRC-17, the odontoid process (atlas centrum) is fused to the axis (Fig. 12C, D). In lateral view, its corpus is anteriorly delimited by a thick ridge that represents the facet for the atlas neural arch. Posterior to it, the corpus of the odontoid process is concave up to the suture with the axis. Ventrally, the odontoid process shows a sagittal suture, indicating the bone is paired (Fig. 12). On both sides, there is an ovoid concavity. The axial rib facet is extending both on the ventrolateral edge of the odontoid as well as on the anterolateral edge of the axis. The axial centrum is longer than deep and, although there is no hypapophysis, its ventral surface bears a faint ridge for its entire length. The neural arch of the axis is poorly preserved as regards the zygapophyses. The neural spine is low and extends for the entire anteroposterior length of the axis.

Cervical Vertebrae—An anterior cervical vertebra (PRC-18) (Fig. 12E, F) is slightly longer than high. No hypapophysis is present but it displays a marked ventral ridge that runs throughout. The parapophysis is distinctly long, representing half of the centrum length. It merges with the anterior facet of the centrum, contrary to the diapophysis, which extends only in the middle of the centrum at the limit with the suture of the neural arch. The diapophysis is long and directed obliquely ventrally. The rest of the neural arch is poorly preserved. Another cervical vertebra from a more posterior position (PRC-959-14) is also longer than high. Here, the ventral surface of the centrum is completely devoid of ridge and is smooth. The parapophysis is still connected to the anterior margin but its section is circular and its proximal process is close to the diapophysis. Both dia- and parapophyses build a wall that

delimits a strong concavity or fossa on the lateral side of the centrum. The anterior and posterior margins are both underlining a markedly concave ventral margin of the centrum.

Thoracal Vertebrae—Two well-preserved thoracal vertebrae (PRC-20 and 21) are connected (Fig. 10I, J). The centra are longer than high and slightly mediolaterally compressed. The ventral margin is concave and devoid of sagittal ridge. The main lateral body of the centrum lacks a fossa. Despite the large size of the vertebrae indicating an adult specimen, the suture of the neural arches with the centrum is apparent and unclosed (Fig. 12). This calls for an investigation of neurocentral suture closure with maturity (Irmis, 2007) in thalattosuchians. The neural spine is about as deep as the centrum and the distal margin is straight and occupies two-thirds of the centrum length. The distal end of the neural spine is thick at mid length and its dorsal surface is flat-to-concave for muscle attachment. The pre- and postzygapophyses slightly extend beyond the anterior and posterior margins of the centrum, respectively. Their orientation is oblique, at 45° from the transverse plane. The transverse process consists of the fused capitulum/tuberculum (the posterior one being twice longer than the anterior one). Their distal end is thick and rounded. The neural canal is ovoid and less than half the diameter of the centrum.

Cervical Ribs—Several elements were found as isolated pieces. One of them (PRC-19) (Fig. 12G, H) is nearly complete and free from the sediment. Its anterior process is broken off at its tip and both anterior and posterior processes seem to be equal in length. The anterior process is flat and the pointed posterior process bears a ridge near the ventral margin. The capitulum is thicker than the tuberculum. The facet of the capitulum for the parapophysis is ovoid and larger than the moon- shaped facet of the tuberculum for the diapophysis.

Appendicular Skeleton

Insights on relative humeral/femoral proportions could not be gathered directly because the recovered elements were mostly disarticulated. However, one humerus was found associated with a complete skull (PRC-239) and one femur was associated with another complete skull (PRC-12) of similar dimensions (Table 1). Assuming no allometric change, a rough humerus/femur ratio is estimated at about 0.63, which falls within the range for other teleosaurids (Mueller-Töwe, 2006).

Scapula—A right scapula (PRC-24) has a proximodistal length of 10.5 cm. The shaft is long and mediolaterally compressed (Fig. 13). The posterior margin of the scapula is straight and remains smooth throughout. It is slightly thicker than the anterior margin of the bone. The laminar scapular distal end is fan-shaped and asymmetric with an anterior projection. This gives to the anterior margin a concave outline. The proximal end of the scapula is thick. Its lateral surface is flat and is delimited anteriorly by a ridge-like acromion process and posteriorly by the thickened supraglenoid buttress. Medially, the corresponding area is smooth and widely convex. The glenoid fossa faces posteroventrally with a slight lateral component. The scapular synchondrosis is rugose and convex and occupies most of the proximal surface.

Humerus—A complete left humerus (PRC-23) is preserved (Fig. 13). It is distinctly long with a proximodistal length of 14.5 cm. The long shaft is rod-like and nearly straight. Proximally, the medial margin expands obliquely, resulting in a wide concave medial margin. The humeral head is thus shifted medially from the rest of the shaft and sends a robust humeral condyle posteriorly. A peg-like medial process is present at the base of the humeral head. On the other side, the deltopectoral crest is faint but clearly visible. It is located away from the humeral head and rests in line with the main shaft. The humerus is squarish in distal view. A pair of shallow supracondylar ridges delimits a shallow, concave surface on the medial margin. The articular surfaces for the radius and ulna are not individualized. On the

opposite side, the lateral and anteromedial epicondylar ridges are acute and extend along the shaft for about 1 cm.

Ilium—A pair of large ilia is preserved (PRC-26 and 28) (Fig. 14) and although the dorsal margin of PRC-26 is slightly eroded, the anterior and posterior processes are intact. The ilium is quadrangular in lateral or medial view. Its anterior margin is slightly deeper than the posterior margin and perpendicularly the dorsal blade is straight. The anterior process is pointed and short and does not extend beyond the level of the anterior peduncle. The acetabulum is wide and shallow and gives to the lateral surface of the bone a wide concave aspect. In proximal view, both peduncles articulating with the ischium are bent laterally. The anterior peduncle is particularly thick and divided in two condyles aligned anteroposteriorly; the anterior-most one articulating with the pubis. The proximal surface of the posterior peduncle is flat and triangular in outline.

Ischium—A right ischium (PRC-27) was found associated with the two ilia (PRC-26 and 28) (Fig. 14). It is nearly complete but has suffered from compression and cracks. The general outline is preserved, with a nearly straight and obliquely oriented posterior margin and a markedly concave anterior margin. The distal end is laminar and has the shape of an axe with an anteriorly projecting process that reaches the level of the anterior process. The acetabular foramen is more notched on the medial side. No pubic process was observed on the anterior process, so the ischium seems to articulate only with the ilium. The anterior process that articulates with the ilium is a rod-like shaft that bends slightly dorsally and projects significantly anteriorly.

Femur—Several femora were recovered. The best preserved (PRC-25 associated to the skull PRC-12) is a left (Fig. 14), but other femora are known (PRC-31 is a very large partial with a proximal width of 4 cm). The femur possesses a distinct sigmoid outline and has a proximodistal length of 17.5 cm and a proximal width of 3 cm. The shaft is mediolaterally

compressed and the distal half of the dorsal surface is narrow and ridge-like As in most crocodylomorphs, the proximal end is mediolaterally compressed, being flat on the lateral side and bearing a knob medially. Along the medial surface of the shaft, the fourth trochanter is faintly expressed as a slightly shallow rugose area, located relatively close to the proximal head. The distal end of the femur is strongly mediolaterally compressed. On the posterior surface of the distal end, a shallow popliteal fossa divides the condyles for the tibia and fibula. There is no intercondylar groove on the anterior surface. The lateral condyle is twice the size of the medial one.

Osteoderms

Disarticulated osteoderms are common at the site. Four osteoderms of the dorsal row were found associated with the skull PRC-8. They connect, the posterior one overlapping the next anterior one. Their outline is subrectangular, being longer than wide. The dorsal side bears a median keel that runs along the entire length of the osteoderm. Large circular pits of variable size ornament the surface. The ventral side is slightly convex and bears a net of fine ridges. The anterolateral edge bears a well-developed spine visible on the last three osteoderms. The anterior margin of the bone next to the spine is not straight but convex. Another dorsal osteoderm (PRC-29, Fig. 15A) is wider than long with a marked anterolateral process. Here, a thick keel runs anteroposteriorly from the level of the anterolateral spine toward the posterior edge. Lateral to the keel, the ornamented surface is laminar and presents a strong convex margin. According to complete shields (e.g., the holotype of *Platysuchus multiscrobiculatus* in Westphal, 1961), osteoderms from the mid-trunk region are wider than long and correspond well with those of PRC-198 — whereas nearly rectangular osteoderms such as those of PRC-8 are observed in the caudal region.

Osteoderms from the ventral shield are identified. The longest suite (PRC-30, Fig. 15B) consists of four partial osteoderms sutured to each other on their medial and lateral margins by strong interdigitating sutures. Each row is overlapped in its anterior margin by another row, thus each osteoderm shows a smooth and anteriorly inclined articular facet. All the osteoderms are wider than long and their external surface is flat and ornamented with large subcircular pits. Their anterior and posterior margins are not straight but undulating.

PHYLOGENETIC ANALYSIS

Indosinosuchus potamosiamensis gen. et sp. nov. and *Machimosaurus hugii* (SMNS 91415) were coded into the matrix of Wilberg (2015a), which was constructed to explore thalattosuchian relationships and includes a total of 78 taxa, including 24 thalattosuchians, and 375 characters. Character codings for *Indosinosuchus potamosiamensis* gen. et sp. nov. and *Machimosaurus hugii* (SMNS 91415) are available in Appendix 1. *Peipehsuchus teleorhinus* Young 1948 from the Ziliunjing Formation of China was coded for the first time by Wilberg (2015a) on the basis of the holotype (IVPP RV 48001) and the complete skull (IVPP RV 10098). However, we highlight in the discussion below that IVPP RV 10098 may not be referable to *P. teleorhinus*. As a consequence, distinguishing the rostrum (IVPP RV 48001) from the complete skull (IVPP RV 10098), we altered three character codings (174, 176 and 184). Moreover, we underline that *Peipehsuchus teleorhinus* is a nomen dubium (see below) and because of its fragmentary condition, the rostrum (IVPP RV 48001) was not included in the phylogenetic analysis. The phylogenetic analysis was performed using TNT (Goloboff et al., 2003) with replicates of 1000 random addition sequences (Wagner trees) followed by a round of TBR branch-swapping. A second round of TBR branch-swapping was

executed using the most parsimonious trees obtained in the first search and stored in the RAM.

In order to further explore the interrelationships of teleosaurids, a smaller matrix incorporating 14 teleosaurids plus *Pelagosaurus typus* as an outgroup taxon was designed for 18 characters (supplementary data). The teleosaurid taxa considered here include *Indosinosuchus potamosiamensis, Lemmysuchus obtusidens, Machimosaurus hugii, Steneosaurus bollensis, Steneosaurus brevior, Steneosaurus durobrivensis, Steneosaurus edwardsi*, *Steneosaurus heberti*, *Steneosaurus leedsi*, *Steneosaurus larteti*, *Steneosaurus priscus*, *Platysuchus multiscobiculatus, Teleosaurus cadomensis* and the Ziliujing teleosaurid. This second analysis was also run in TNT with the parameters mentioned above.

Results

The original analysis of Wilberg (2015a) yielded 10 most parsimonious trees (MPTs) of length 1654. The addition of *Indosinosuchus potamosiamensis* gen. et sp. nov. did not change the number of MPTs but did add a total of 12 steps (1666). The strict consensus topology is similar to that of Wilberg (2015a) with a monolophyletic Thalattosuchia positioned near the base of Crocodylomorpha (Fig. 16). Within Teleosauroidea, *Indosinosuchus potamosiamensis* and *Machimosaurus hugii* are recovered as sister taxa within a broader group that includes IVPP RV 10098 and the Middle Jurassic pair *Steneosaurus leedsi* and *Steneosaurus durobrivensis*; *Steneosaurus larteti* is basal to this group. Another main group consists of the Middle Jurassic *Teleosaurus cadomensis* recovered basal to the early Jurassic *Pelagosaurus typus* and then to the early Jurassic pair *Platysuchus multiscrobiculatus* + *Steneosaurus bollensis*. All the above-mentioned taxa are recovered in a sister taxon relationship to the Middle Jurassic *Steneosaurus brevior* + *Steneosaurus brevidens*. Although the topology is well resolved, stratigraphic inconsistencies are present

and the deep nesting of *P. typus* within teleosaurids is dubious given contradicting hypotheses based on character discussion or phylogenetic analyses placing *P. typus* either with teleosaurids or with metriorhynchids (e.g. Buffetaut, 1982; review in Pierce and Benton, 2006; Young et al. 2012; Wilberg, 2015a, b). The organization of Metriorhynchoidea has not changed and they are confirmed as sister to teleosaurids.

The second, more exclusive, analysis yielded a single MPT of 43 steps. The general topology within teleosaurids is slightly different with *S. bollensis* as the basal-most taxon but the new Thai taxon is recovered in a deeply nested position, as in the previous analysis (see below for a detailed discussion).

DISCUSSION

Affinities and Comparisons

Resolving teleosaurid relationships remains challenging because of several factors including preservation and the high degree of anatomical convergence involving several characters, notably linked to snout elongation. Although their fossil record is rich and often represented by complete and articulated specimens (e.g. Westphal, 1962; Mueller-Töwe, 2006), teleosaurid skeletons preserved in shales or mudstones are often crushed and their anatomical connection hampers complete observations of their anatomy. Teleosaurid topologies are often characterized by disparate internal branchings (compare results in Jouve, 2009; Herrera et al., 2015 or Wilberg, 2015b). In addition, anatomical convergence in a clade exclusively composed of longirostrine taxa adds substantial noise for establishing diagnostic characters. In order to tackle species delineation, attempts have experimented with morphometric methods (Adams-Tresman, 1987; Pierce et al., 2009) but teleosaurid intrarelationships remain tentative. According to current consensus, a monophyletic

Teleosauridae excludes *Pelagosaurus typus*, which is considered a Thalattosuchia *incertae sedis* (Pierce and Benton, 2006) and resolved at the base of Metriorhynchoidea (e.g. Young et al. 2012; Wilberg, 2015b). The most recent phylogenetic investigations that include teleosaurids are aimed at exploring the position of Thalattosuchia within Crocodylomorpha (Wilberg, 2015b) or resolving metriorhynchoid relationships (e.g. Young et al., 2012; Herrerra et al., 2015). Many recent analyses include teleosaurids with a similar species count (n = 5 in Jouve, 2009; n = 9 in Young et al., 2012; n = 8 in Martin and Vincent, 2013; n = 9 in Herrerra et al., 2015 or Wilberg, 2015b; n = 11 in Fanti et al. 2016). Fluctuations in species content reflect whether *Machimosaurus* is considered mono- (Martin et al., 2015) or plurispecific (up to n = 4 in Fanti et al., 2016). Nevertheless, all these analyses (Young et al., 2012; Martin and Vincent, 2013; Herrerra et al., 2015; Wilberg, 2015a, b; Fanti et al., 2016) consistently recover teleosaurids as monophyletic.

Here, *Indosinosuchus potamosiamensis* gen. et sp. nov. is unambiguously resolved within Teleosauridae (Fig. 16A). The present result, using the matrix of Wilberg (2015a) confirms a previous result (Martin et al., 2016) using the earlier matrix of Young et al. (2009). The inclusion of *Indosinosuchus potamosiamensis* gen. et sp. nov. in Teleosauridae is supported by the presence of the following synapomorphies: skull roof with large supratemporal fenestrae, lateral margins of supratemporal arches located below level of sagittal crest, squamosal devoid of ornamentation, anterior processes of nasals do not reach premaxillae, postorbital longer than squamosal, long mandibular symphysis involving splenials, pendulous and bifid basioccipial tubera. The recovery of *Pelagosaurus typus* deeply nested among teleosaurids contradicts recent hypotheses proposing a sister group position to Teleosauridae and Metriorhynchidae (Clark, 1994) or recovering it as the basal-most metriorhynchoid (e.g. Young et al., 2012; Wilberg, 2015b).

Restricting the ingroup to teleosaurids and forcing *Pelagosaurus typus* to be the teleosaurid outgroup, produces an alternative phylogenetic topology. Here, one tree of 43 steps was recovered (Fig. 16B). *Steneosaurus* is not monophyletic and more work will be needed to define what constitutes *Steneosaurus*. Among the most deeply nested teleosaurids, IVPP RV 10098 is recovered a sister to the exclusive clade of *Steneosaurus durobrivensis* and *Lemmysuchus obtusidens*; they are collectively united by nasals shorter than the supratemporal fenestrae (ch. 3) and a parietal restricted to the posterior margin of the skull roof (ch. 13). The sister group to this clade is *Machimosaurus hugii* and *Steneosaurus priscus*, lineage which is diagnosed by the absence of an antorbital fenestra (ch. 2) and by small orbits relative to the interorbital width (ch. 1). An absence of antorbital fenestra characterizes other taxa such as *Lemmysuchus obtusidens*, *Steneosaurus durobrivensis*, *Steneosaurus edwardsi* and *Steneosaurus heberti*, which are not closely related according to the present hypothesis. This analysis therefore does not support the monophyletic Machimosaurini recently proposed by Jouve et al. (2016) to include *Machimosaurus* and *L. obtusidens* — unless *Steneosaurus priscus* and IVPP RV 10098 are also included. According to the present results, *Indosinosuchus potamosiamensis* is recovered basal to the aforementioned group, all of them characterized by an external mandibular fenestra with equally tall anterior and posterior margins (ch. 17). The clade containing *Steneosaurus brevior*, *Platysuchus multiscrobiculatus* and *Teleosaurus cadomensis* is characterized by a supratemporal fenestrae whose length is subequal to its width (ch. 6). Both this clade and the clade including *Indosinosuchus potamosiamensis* are united by laterally expanded premaxillae (ch. 8). *Steneosaurus larteti*, *Steneosaurus heberti* + *Steneosaurus edwardsi* and *Steneosaurus leedsi* represent successive sister groups with premaxillae in line with the rest of the rostrum. The basal-most teleosaurid is *S. bollensis*, which is the only teleosaurid possessing subrectangular dorsal osteoderms (ch. 16), a condition shared with *Pelagosaurus typus*.

Here, further discussion is based on comparative anatomy, involving similarities and differences that are not necessarily included in the datamatrix. In comparison to other teleosaurids, the Phu Noi teleosaurid has a rostrum to skull length ratio of 0.66 and can be qualified as falling in a group of teleosaurids with a moderately elongated rostrum such as *Steneosaurus brevior*, *Steneosaurus edwardsi*, *Steneosaurus durobrivensis, Steneosaurus obtusidens* and *Machimosaurus hugii*. *Steneosaurus larteti* and *Steneosaurus heberti* have comparable ratios but their rostrum is much slender. All other teleosaurids known from complete skulls have a slender and more elongate rostrum with a ratio of circa 0.75 and above such as *Teleosaurus cadomensis*, *Steneosaurus bollensis*, *Steneosaurus gracilirostris*, *Steneosaurus leedsi*, specimen IVPP RV 10098) and *Platysuchus multiscrobiculatus*.

As in most teleosaurids, the premaxillae of the new Thai taxon are moderately expanded laterally. This expansion is variably expressed and is prominent in taxa such as *Teleosaurus cadomensis* according to the reconstruction provided by Eudes-Deslongchamps (1870), *Platysuchus multiscrobiculatus* (see holotype in Westphal, 1961), and IVPP RV 10098 referred to *Peipehsuchus teleorhinus* by Li (1993). Exceptions include *Steneosaurus bollensis*, *Steneosaurus gracilirostris* and *Steneosaurus leedsi* where the lateral margin of the premaxilla is nearly aligned with that of the maxilla.

The Thai taxon possesses 4 premaxillary alveoli, as in IVPP RV 10098, *Steneosaurus megistorhynchus*, *Steneosaurus leedsi*, *Steneosaurus larteti* and *Steneosaurus durobrivensis* (Eudes-Deslongchamps, 1870; Andrews, 1913; Godefroit, 1995). Eudes-Deslongchamps (1870) reconstructs four to five alveoli per premaxilla in *Teleosaurus cadomensis*. Other teleosaurids possess three alveoli per premaxilla such as *Machimosaurus hugii*, *Steneosaurus heberti*, *Steneosaurus gracilirostris*, *Platysuchus multiscrobiculatus*, *Steneosaurus brevior* (Buffetaut, 1982; Martin and Vincent, 2013; Morel de Glasville, 1876; Mueller-Towe, 2006).

The premaxillary alveolar count is variable in *Steneosaurus bollensis* with 3 to 4 alveoli according to Mueller-Towe (2006).

The Thai taxon possesses 30 maxillary alveoli, a count which falls in the range observed for *Steneosaurus bollensis* (26–35 according to Mueller-Towe, 2006). Teleosaurids with a smaller maxillary alveolar count include the mesorostrines *Machimosaurus hugii* (22) and *Steneosaurus brevior* (25) (Mueller-Towe, 2006; Martin and Vincent, 2013), *Steneosaurus edwardsi* (23) (Eudes-Deslongchamps, 1863–1867) or IVPP RV 10098 (27) whereas all other teleosaurids with longer rostra have more than 30 maxillary alveoli such as *Teleosaurus cadomensis* (45 according to the reconstruction of Eudes-Deslongchamps, 1870), *Steneosaurus gracilirostris* (45–57, Mueller-Towe, 2006), *Steneosaurus leedsi* (41–42, Andrews, 1913), *Platysuchus multiscrobiculatus* (30–40, Mueller-Towe, 2006), *Steneosaurus larteti* (32 according to the reconstruction of Eudes-Deslongchamps, 1870), *Steneosaurus heberti* (36, Morel de Glasville, 1876), and *Steneosaurus durobrivensis* (30, Andrews, 1913).

As in several teleosaurids, the anterior margin of the supratemporal fenestra, as seen in dorsal view, is perpendicular to the sagittal plane. The same anterior margin in *Steneosaurus leedsi*, *Steneosaurus heberti* and *Steneosaurus durobrivensis* is gently convex. *Platysuchus multiscrobiculatus* is unique in having a strongly oblique anterior margin of the supratemporal fenestra.

The Thai taxon is similar to many teleosaurids in having supratemporal fenestrae whose length is nearly twice its width; these include *Steneosaurus leedsi*, *Steneosaurus larteti*, *Steneosaurus heberti*, *Steneosaurus durobrivensis* and *Machimosaurus hugii*. On the contrary, the fenestrae are only slightly longer than wide in *Steneosaurus brevior*, *Steneosaurus gracilirostris*, *Steneosaurus bollensis* and as long as wide in *Teleosaurus cadomensis* and *Platysuchus multiscrobiculatus*.

The main results of the phylogenetic analyses concerning *Indosinosuchus potamosiamensis* are: 1) this new taxon is unambiguously recovered within Teleosauridae; and 2) it does not form an exclusive clade with the Ziliujing teleosaurid IVPP RV 10098. Further details on the systematics of the Chinese form are detailed below.

Peipehsuchus teleorhinus and the Phu Noi Teleosaurid

Proving the Phu Noi teleosaurid is or is not distinct from *Peipehsuchus* is difficult due to the poor preservation of the holotype of *Peipehsuchus teleorhinus* (IVPP RV 48001) and because we are not certain that material referred to this taxon (Li, 1993) is really conspecific (see below).

The holotype IVPP RV 48001 consists of the anterior part of a rostrum with premaxillae and the anterior part of the maxillae preserved up to the level of the sixth alveoli (Fig. 17A–C). This specimen displays forward facing external nares, premaxillae enclosing the external nares, three premaxillary alveoli, widely spaced and similarly sized maxillary alveoli, a marked premaxillary-maxillary embayment. All these characters, even used in combination are commonly observed among teleosaurids and do not validate a distinct species. We therefore consider *Peipehsuchus teleorhinus* a *nomen dubium*.

Li (1993) described a complete skull that she referred to *P. teleorhinus*. However, it is unclear whether both specimens come from the same locality and even from the same stratigraphic level (see discussion below on the age of teleosaurids from Asia). Moreover, on what is comparable, the number and size proportions of premaxillary alveoli of the holotype differ from those in the premaxilla of the complete skull (IVPP RV 10098) (Fig. 17D). In IVPP RV 10098, the premaxilla possesses four alveoli, the first two being contiguous and positioned close to the median premaxillary suture. Noteworthy are the different profiles of the premaxillae in those two specimens: in the holotype, the premaxilla is as long as wide in

ventral view with the last two premaxillary alveoli aligned; on the other hand in IVPP RV 10098, the premaxilla is wider than long with the last; i.e., the fourth, premaxillary alveolus shifted laterally from the third premaxillary alveolus. Admittedly, the premaxillae of the holotype are not well preserved and the observed difference in outline may reflect damage of the lateral rims of the premaxillae that would have extensively eroded the alveolar margins of the last premaxillary alveoli in the holotype. Due to the poor preservation of the holotype, the apparently different morphology observed in IVPP RV 10098, and uncertainties concerning the geographical and stratigraphical location of the holotype, we question the assignation of IVPP RV 10098 to the same species as IVPP RV 48001.

Restricting our comparison to the holotype IVPP RV 48001, none of the specimens from the Phu Noi locality could be assigned to *Peipehsuchus teleorhinus* based on at least two characters. In all Thai specimens and contrary to IVPP RV 48001, the premaxilla possesses four alveoli, not three; and in dorsal view, the posterior margin of the external nares is concave, not convex. A premaxillary alveolar count differing by one alveolus may be population-level variation but none of the six skulls preserving the premaxillae possess three alveoli: they all have four. It could also be argued that the outline of the external nares may be affected by deformation. Again, in the six skulls from Phu Noi where complete premaxillae are preserved under variable sedimentary compression, all display a concave posterior margin of the external nares suggesting that the material from Phu Noi is not comparable to IVPP RV 48001.

Comparing the Phu Noi specimens with specimen IVPP RV 10098 is more convenient due to its relative completeness. Overall, many similarities have been noted (Martin et al. 2016) and they both share (1) the presence of a relatively large and slit-like antorbital fenestra bordered dorsally by the lacrimal; (2) the nasals excluded from the narial border; (3) the same premaxillary alveolar counts with 4 alveoli; and (4) longer than wide supratemporal fenestrae.

In addition to their different phylogenetic positions, several differences are also pinpointed here and include: (1) the general morphology of the premaxilla, which is laterally expanded in IVPP RV 10098 versus as long as wide in the Thai taxon (although dorsoventral compression may alter its outline); (2) the relative position of the last premaxillary alveolus, which is shifted laterally and is the largest in IVPP RV 10098 but is aligned with the third and of similar diameter in the Thai taxon; (3) a different maxillary alveolar count with 30 alveoli for the Thai taxon versus 27 for IVPP RV 10098; (4) a short anterior nasal process in IVPP RV 10098, reaching the 18th maxillary alveolus but a longer and pinched processes in the Thai taxon, reaching the 14-15th maxillary alveolus; (5) short posterior processes of the nasals not reaching the anterior margin of the orbits in IVPP RV 10098. In the Thai taxon, however, comparatively longer posterior processes of nasals almost reaching the medial orbital margin and nearly preventing a contact between prefrontals and frontal; (6) in dorsal view, the parietal is restricted to a short triangle on the posteromedian area of the skull roof in IVPP RV 10098 but it extends as a long triangle between the supratemporal fenestrae in the Thai taxon; (7) rostrum to skull length ratio indicates a long rostrum (0.74) in IVPP RV 10098 versus a relatively shorter rostrum in the Phu Noi teleosaurid (0.66 ± 0.02 2SD for n = 5); (8) more marked premaxillary-maxillary festooning in IVPP RV 10098 by comparison to the Thai material.

We conclude that the Thai material cannot be assigned to the same taxon as the holotype of *Peipehsuchus teleorhinus*, here considered a *nomen dubium*. Hence, the new taxon name, *Indosinosuchus potamosiamensis* gen. et sp. nov. is proposed for the material from the Jurassic of Phu Noi, northeastern Thailand. Furthermore and as detailed above, the complete skull IVPP RV 10098 is different from the new Thai teleosaurid and its systematic position will have to be reassessed in a future study.

The Age of Phu Noi and the Stratigraphic Range of Asiatic Teleosaurids

The continental nature of the Phu Kradung formation and the absence of volcanic ash do not help to assess precise ages for the different fossiliferous localities. Therefore, their age, including the locality of Phu Noi, within this formation remains difficult to constrain within a Jurassic/lower Cretaceous time frame. Fossil vertebrates discovered at various localities in the Phu Kradung Formation seem to indicate a Late Jurassic age (Buffetaut et al., 2001; Buffetaut and Suteethorn, 2007; Tong et al., 2009) but palynomorphs from outcrops near Hui Sai and Nong Bua Lamphu (Racey and Goodall, 2009) and detrital zircons (Carter and Bristow, 2003) may indicate an Early Cretaceous age. Although palynological analyses point to an Early Cretaceous age for the Phu Kradung Formation, a Late Jurassic age for its lower part could not be ruled out by Racey and Goodall (2009). In the case of Phu Noi, because the locality is located within the lower part of the Phu Kradung Formation, a Late Jurassic (?Tithonian) age was recently proposed (Liard and Martin, 2011; Cuny et al., 2014; Liard et al., 2015; Deesri et al., 2014; Martin et al., 2016). Nevertheless, the age of Phu Noi is not settled, in part because most of its faunal content is still under study since the discovery of the site in 2008. Therefore, a preliminary account regarding their biostratigraphical significance is given below.

Cuny et al. (2014) reported numerous hybodont microremains at Phu Noi, including *Acrodus* known from Triassic and Jurassic deposits (Rees and Underwood, 2006), *Jaiodontus* known from the Oxfordian of China (Klug 2010), as well as dermal denticles similar to denticles from the Bathonian–Callovian Khlong Min Formation of Peninsular Thailand. Moreover, the absence of *Heteroptychodus* at Phu Noi, otherwise known from younger levels of the Phu Kradung Formation such as the possibly Early Cretaceous locality of Kham Phok, support a Late Jurassic age for the Phu Noi locality (Cuny et al., 2014). Ginglymodian fishes

are abundant at Phu Noi (Deesri et al., 2014; 2016) but their stratigraphic range is too extensive (Triassic–Present) to be age definitive.

Temnospondyl vertebrae are present at Phu Noi and were previously reported from the Phu Kradung Formation at Nam Nao on the Khorat Plateau of northeastern Thailand (Buffetaut et al., 1994b) as well as from the Jurassic of Mab Ching, Peninsular Thailand — part of the Khlong Min Formation (Buffetaut et al., 1994a). The Khlong Min Formation belongs to the Shan-Thai block whereas the Phu Kradung Formation is part of the Indochina block. The Khlong Min Formation may be considered Middle or Late Jurassic in age (Buffetaut et al., 2005) and more specifically Bathonian–Callovian according to Cuny et al. (2014). Although temnospondyls occur in the Middle Jurassic of China (Maisch and Matzke, 2005), they are also present in other Cretaceous Laurasian and Gondwanan localities (Warren et al., 2000) and therefore cannot significantly constrain the age of Phu Noi.

The turtle assemblage from Phu Noi, represented by xinjiangchelyids such as *Phunoichelys thirakhupti* (Tong et al., 2015) and another as-yet-undescribed xinjiangchelyid, is distinct from other assemblages placed in the upper part of the Phu Kradung Formation, which include abundant remains of trionychoid turtles such as *Basilochelys macrobios* (Tong et al., 2009). Known since the Middle Jurassic, xinjiangchelyids are a dominant turtle group in the Late Jurassic of Asia (Central Asia and China), whereas records of this group in Early Cretaceous deposits are scarce in mainland Asia. This is represented by a single shell from the Tugulu Group in Xinjiang, China (Danilov and Parham, 2007). Xinjiangchelyid remains were reported from the Early Cretaceous Tetori Group of Japan. However, the Japanese turtle assemblages include also more deeply nested Eucryptodira sinemydids/macrobaenids and crown-group trionychoids (Hirayama, 2006). It is noteworthy that xinjiangchelyids from the Tetori Group have more derived chacters than those from Phu Noi. Although several taxa from the Early Cretaceous of Europe were attributed to Xinjiangchelyidae (see Perez-Garcia

et al., 2017), with an age ranging from Hauterivian to Aptian; morphologically, the xinjiangchelyid turtles from Phu Noi appear to be closer to those from China than those from Europe. The turtle assemblage from Phu Noi, which is exclusively composed of xinjiangchelyids is also more comparable to those from the Late Jurassic of China, whereas in the Early Cretaceous turtle assemblages of Japan, xinjiangchelyids are found with more deeply nested turtles such as trionychoids and sinemydids (Hirayama, 2006).

Teleosaurids are common in marine deposits from the Toarcian to the Tithonian, the most complete record being from Western Europe (e.g. Andrews, 1909; Westphal, 1961). Evidence for the presence of teleosaurids in Cretaceous deposits concerns two specimens. The first was reported by Cornée and Buffetaut (1979) as *Steneosaurus* sp. from the Valanginian of southern France but the specimen is now referred to Plesiosuchina indet., a metriorhynchoid (Young et al., 2014). A second specimen of Cretaceous teleosaurid was recently described as a new species of *Machimosaurus*, *M. rex*, from the Hauterivian Douiret Formation of Tunisia (Fanti et al., 2016). Unfortunately, the locality age is poorly constrained: the pycnodont *Gyrodus* is difficult to identify based on isolated teeth (Cuny et al., 2010) and the hybodont *Egertonodus* first appears in the Bathonian (Rees and Underwood, 2008). Therefore, there is no compelling evidence for the survival of teleosaurids in the Cretaceous. Teleosaurid remains were mentioned from Peninsular Thailand at various localities (Cuny et al., 2009; Buffetaut et al., 1994c) in the Jurassic Khlong Min Formation.

Mamenchisaurid sauropod remains are abundant at Phu Noi but provide ambiguous information because of their stratigraphic range from the Early Jurassic to Early Cretaceous (Suteethorn et al., 2013; Xing et al., 2015). The ornithopod reported from Phu Noi may be comparable to other taxa known from Jurassic and Cretaceous deposits worldwide (Buffetaut et al., 2014) and until a comprehensive description is provided, cannot be used to sort out a particular age. Sinraptorid theropods, which are known from the Jurassic Shishugou and

Shaximiao Formations of China (Currie and Zhao, 1993; Dong et al., 1978; 1983), were briefly mentioned at Phu Noi (Chanthasit, 2011; Buffetaut et al., 2014). But their presence provides an ambiguous age interpretation because a sinraptorid tibia was reported from the upper part of the Phu Kradung Formation at Kham Phok (Buffetaut and Suteethorn, 2007), a locality recently interpreted as possibly coeval with the potentially Early Cretaceous locality of Nong Bua Lamphu (Racey and Goodall, 2009) based on the proximity of the overlying Phra Wihan Formation and the shared occurrence of the pholidosaurid *Chalawan thailandicus* at both sites (Martin et al., 2014b). A stegosaurid vertebra was discovered from the locality of Khok Sanam (Buffetaut et al., 2001), which belongs to the lower part of the Phu Kradung Formation and is geographically close to the locality of Phu Noi. Although stegosaurids are common in Jurassic deposits worldwide, they are also known from the Early Cretaceous in China (Dong, 1973).

According to the above-listed faunal occurrences, a preliminary age is proposed but alternative interpretations may arise with more detailed faunal descriptions. Although dinosaurs provide ambiguous age information for Phu Noi, the presence of the hybodont *Acrodus* and of teleosaurids seem to exclude a Cretaceous age for Phu Noi. More precisely, the hybodont genus *Jaiodontus* and the peculiar hybodont dermal denticles may point to a Bathonian-Oxfordian interval whereas xinjiangchelyid turtles seem to favor a Late Jurassic age. Although temnospondyls survive into the Cretaceous, their presence at Phu Noi and in the Middle Jurassic of the Junggar Basin, China should be kept in mind. Therefore, Phu Noi locality may be Middle to Late Jurassic in age.

The holotype of *Peipehsuchus teleorhinus* (IVPP RV 48001) and the complete skull (IVPP RV 10098) described by Li (1993) were recovered from the Ziliujing Formation of Sichuan, China. There is some uncertainty about the provenance of the holotype with Young (1948) placing it in the Da'anzhai Member of the Ziliujing Formation whereas Dong (1984)

placed it in the underlying Ma'anshan member of the Ziliujing Formation. The referred complete skull (IVPP RV 10098) is from Daxian, Sichuan Province, Ziliujing Formation although the exact stratigraphic level is unknown (Li, 1993 p. 90) but could be from the same level as IVPP RV 48001 (Li, 1993 p.85). The Da'anzhai Member was considered Early Jurassic by Peng et al. (2005) on the basis of ostracods, bivalves and pollen content as well as on the occurrence of the prosauropod cf. *Lufengosaurus magnus*. A recent review of the sauropod *Sanpasaurus yaoi* from the Ziliujing Formation emphasizes the age of the Ma'anshan Member could be Early Jurassic and that the Da'anzhai Member could be early Middle Jurassic (McPhee et al., 2016). Therefore, teleosaurids from the Ziliujing Formation could be Early to Middle Jurassic in age.

In conclusion, teleosaurids may have been present in freshwater drainages of Asia during most of the Jurassic with the Ziliujing teleosaurids from the Early/Middle Jurassic, teleosaurids from Peninsular Thailand from the Middle Jurassic and the new Thai taxon from Phu Noi *Indosinosuchus potamosiamensis* from the Middle to Late Jurassic. This fossil record markedly contrasts with that from Europe at the same time, where teleosaurids are primarily recovered from marine deposits. This fossil record may also be biased because the record in Asia is less well known for marine reptiles in comparison to Europe; and alternatively the tetrapod continental record is rather good in Asia. Geographically intermediate occurrences of teleosaurids are scarce. In a brief report, a teleosaurid skull possessing a small antorbital fenestra from the Aalenian Karakh Formation of Dagestan was presented as *Steneosaurus* sp. (Efimov, 1982; 1988). Although underlying Toarcian levels contain abundant ammonites, Krymholts and Mesezhnikov (1988) indicate that the Karakh Formation includes sandstone, siltstone, mudstone and locally coal. So it is not clear whether *Steneosaurus* sp. from Dagestan was recovered from a marine, continental or transitional environment. Although not figured, Efimov and Chkhikvadze (1987) report a tooth crown of *Teleosaurus* sp. from the

uppermost Jurassic/lower Cretaceous of the Fergana Basin, Kyrgystan, but the nature of the deposit is unknown. The morphology and affinities of teleosaurids from Central Asia are therefore virtually unknown.

Taphonomy and Preservation

Two individuals (PRC-8 and KS33-209) were surface-collected during early prospections of the Phu Noi hill so their precise stratigraphic provenance in the locality is unknown. The subsequent recovery, from a single horizon containing abundant fish, turtle and dinosaur remains, of the 8 other teleosaurid individuals, which encompass different size categories with juvenile, subadult and adult individuals, raises questions about the cause of their death. The lower part of the Phu Kradung Formation has been interpreted as a lake-dominated floodplain with meandering and braided river channel deposits (Racey and Goodall, 2009). Locally at Phu Noi, the main fossiliferous layer was reconstructed as part of an abandoned channel or as an oxbow lake, part of a complex river system (Cuny et al., 2014; Liard et al., 2015).

Small and delicate (e.g., teleosaurid limb bones) as well as large bones (e.g., sauropod bones) are scattered over the excavation surface. At least six fish skeletons of different sizes were recovered in this horizon, one including part of its body and two of them being nearly complete (Deesri, pers. obs.). A small turtle (currently under study) had its skull lying on the external surface of the articulated carapace. All these features imply minimal transport following skeletal disarticulation. Additional taphonomical details are noted below as they concern teleosaurids and may be used in future studies to help tease apart the taphonomic and paleoenvironmental context of the assemblage.

Beardmore et al. (2012) studied articulation patterns and preservation in *Steneosaurus* skeletons from the Lower Jurassic of Germany. Although both articulated and disarticulated

specimens are represented in their dataset, skulls and mandibles are often recovered maintaining close anatomical position with the rest of the postcranium. The Holzmaden fauna was deposited in a marine anoxic environment with limited bottom currents whereas the Phu Noi assemblage was deposited in a freshwater habitat potentially subjected to floods and droughts. In Phu Noi and contrary to Holzmaden, none of the skulls retain articulation with the cervical vertebrae. In Phu Noi, five skulls are preserved with the articulated (PRC-239, PRC-238, KS-33-209) or nearly articulated mandibles (PRC-11, PRC-240). Three other skulls were recovered without a mandible (PRC-8, PRC-9, PRC-10) and one skull was recovered with its broken mandibular rami placed over the top of the skull and postcranial elements scattered around it (PRC-12). The observed degree of skeletal disarticulation at Phu Noi implies limited transport on a short distance after carcasses had decayed, with possible scattering by scavengers.

A nearly complete teleosaurid vertebral column shows a strong backward flexure of the cervical region and is missing the skull, ribs, caudal series of vertebrae, and appendicular elements (PRC-22, Figure 12K). This specimen is comparable in its arrangement to carcasses of *Crocodylus porosus* retrieved from the taphonomic experiment of Syme and Salisbury (2014). These authors characterize an advanced stage of decay with the heavy skull hanging below the body (see their Fig. 7), eventually detaching from the floating carcass together with appendicular elements and ribs. Given the marked U-shaped profile of PRC-963 and the absence of cranial and appendicular elements in its vicinity, it is likely that this specimen bloated and floated. Syme and Salisbury (2014) observed that further decay under subaqueous conditions led to near-or-total disarticulation of the skeleton, but this is not the case in PRC-22, which maintains connection between cervical, thoracic and sacral vertebrae. Either burial interrupted the decaying process or extensive subaerial drying of the carcass maintained vertebral units with tendons or muscles preserving the integrity of the articulated column.

Other observations may support the latter hypothesis. Liard et al. (2015) noted the presence of desiccation cracks at the base of the bonebed implying temporary subaerial exposure of the deposit. Prolonged subaerial exposure is also supported by rosette-type marks on the surface of some sauropod ribs (Martin et al., 2016) attributable to pupation chambers of dermestid beetles or similar insects (Bader et al. 2009). We also observed such marks on the skull surface of two teleosaurids at Phu Noi (Fig. 18). Their presence implies that carcasses with decaying flesh reached a dry stage in order to become available to necrophagous dermestids to lay eggs. As described by Bader et al. (2009), about 8 weeks elapse between egg laying and hatching in dermestids. Because such arthropods are exclusively terrestrial, this implies that the carcasses were not submerged for at least that time span. Moreover, those insects only develop in the dry season because wet conditions with mold development kill them (Timm, 1982; Bader et al., 2009). Therefore, not only sauropod carcasses decayed subaerially at Phu Noi; teleosaurid carcasses were also drying in a terrestrial and dry atmosphere permitting the development of the dermestid pupae.

The most probable sequence of events implies that teleosaurids died in the aquatic environment and were eventually exposed to further subaerial decay. This hypothesis is both compatible with a major drought where aquatic animals would find temporary refuge in water holes and would die with food resources becoming rare. This has been observed in modern-day ecosystems with *Crocodylus niloticus* congregating during drought years (Kofron, 1993). Also possible is a flash flood event, a scenario proposed for the formation of dinosaur bonebeds in North America (Eberth, 2015), drowning the majority of organisms recovered at Phu Noi. Trapped organisms would have started to decay in water and would have continued their decomposition subaerially. Weeks or months later, a subsequent rise in water level would have deposited fine silts, burying and preserving everything.

Conclusions

The discovery of several teleosaurid individuals at a single locality in a Jurassic continental deposit from northeastern Thailand is important for the following reasons. First, it underlines obvious faunal changes in the composition of Mesozoic freshwater faunas with the presence of thalattosuchians in freshwater drainages during the Jurassic. These forms were replaced in the Cretaceous by goniopholidids (Lauprasert et al., 2007) and pholidosaurids (Martin et al. 2014b). Second, it indicates teleosaurids were ecologically versatile, setting the stage for interesting future studies that explore the freshwater versus marine adaptations in this group. Teleosaurids are indeed abundant and represented by complete skeletons in European formations such as the Posidonia Shale in Germany, the Oxford Clay in the UK, and les Vaches Noires in France, indisputably reflecting their marine lifestyle. But whether we are missing a part of their life cycle in the brackish and/or freshwater habitats remains an open question. For example, the co-occurrence of teleosaurids and abundant sauropod remains in Middle Jurassic brackish-to-continental deposits at El Mers in Morocco (Lapparent, 1955; Charrière et al., 1994) indicates a potential mixture of vertebrate remains with allochtonous origin. Further work is needed to understand whether freshwater adaptations in teleosaurids are plesiomorphic or derived (see discussion in Martin et al., 2016). As recently proposed (Wilberg, 2015a), our work considers a possible Triassic origin of thalattosuchians among land-dwelling forms, which may help understand the sudden abundance of teleosaurids in marine deposits of the Early Jurassic (Toarcian). Fieldwork will have to focus on freshwater deposits of the Hettangian and Pliensbachian in the search for transitional forms.

ACKNOWLEDGMENTS

We thank students and members of the Palaeontological Research and Education Centre (PRC) of Mahasarakham University, T. Liard and P. Chantasit and other members of the staff of Sirindhorn Museum and of Department of Mineral Resources (DMR) of Thailand for their support in the field. The project was supported by a research grant from Mahasarakham University and by the National Research Council of Thailand (NRCT 269821). This research is supported by the project PalBioDivASE under a "Groupe de Recherche International" (GDRI) grant from CNRS. JEM thanks L. Cavin, G. Cuny and R. Allain for discussions. We thank the editor G. Bever, D. Pol, and one anonymous reviewer, whose comments helped improve the initial version of this manuscript.

LITERATURE CITED

Adams-Tresman, S. M. 1987. The Callovian (Middle Jurassic) teleosaurid marine crocodiles from central England. Palaeontology 30:195–206.

Andrews, C. W. 1909. On some new *Steneosaurus* from the Oxford Clay of Peterborough. Annals and Magazine of Natural History 3:299–308.

Andrews, C. W. 1913. A Descriptive Catalogue of the Marine Reptiles of the Oxford Clay, Part Two. British Museum (Natural History), London, 206 pp.

Bader, K. S., S. T. Hasiotis, and L. D. Martin. 2009. Application of forensic science techniques to trace fossils on dinosaur bones from a quarry in the upper Jurassic Morrison Formation, northeastern Wyoming. Palaios 24:140–158.

Beardmore, S. R., P. J. Orr, T. Manzocchi, and H. Furrer. 2012. Float or sink: modeling the taphonomic pathway of marine crocodiles (Mesoeucrocodylia, Thalattosuchia) during the death–burial interval. Palaeobiodiversity and Palaeoenvironments 92:83–98.

Benson, R. B., and R. J. Butler. 2011. Uncovering the diversification history of marine

tetrapods: ecology influences the effect of geological sampling biases. Geological Society of London Special Publications 358:191–208.

Brusatte, S. L., A. Muir, M. T. Young, S. Walsh, L. Steel, and L. M. Witmer. 2016. The braincase and neurosensory anatomy of an Early Jurassic marine crocodylomorph: Implications for crocodylian sinus evolution and sensory transitions. The Anatomical Record 299:1511–1530.

Buffetaut, E. 1982. Radiation évolutive, paléoécologie et biogeographie des crocodiliens mésosuchiens. Mémoires de la Société Géologique de France 142:1–88.

Buffetaut, E., and V. Suteethorn. 2007. A sinraptorid theropod (Dinosauria: Saurischia) from the Phu Kradung Formation of northeastern Thailand. Bulletin de la Société Géologique de France 178:497–502.

Buffetaut, E., V. Suteethorn, and H. Tong. 2001. The first thyreophoran dinosaur from Southeast Asia: a stegosaur vertebra from the Late Jurassic Phu Kradung Formation of Thailand. Neues Jahrbuch für Geologie und Paläontologie Monatshefte 2:95–102.

Buffetaut, E., V. Suteethorn, H., Tong, and A. Košir, A. 2005. First dinosaur from the Shan–Thai Block of SE Asia: a Jurassic sauropod from the southern peninsula of Thailand. Journal of the Geological Society 162:481-484.

Buffetaut, E., G. Termier, and H. Termier. 1981. A teleosaurid (Crocodylia, Mesosuchia) fromthe Toarcian of Madagascar and its palaeogeographical significance. Paläontologische Zeitschrift 55:313–319.

Buffetaut, E., L. Raksaskulwong, V. Suteethorn, and H. Tong. 1994a. First post-Triassic temnospondyl amphibians from the Shan-Thai block: intercentra from the Jurassic of peninsular Thailand. Geological Magazine 131:837–839.

Buffetaut, E., H. Tong, and V. Suteethorn. 1994b. First post-Triassic labyrinthodont amphibian in South East Asia: a temnospondyl intercentrum from the Jurassic of

Thailand. Neues Jahrbuch für Geologie und Paläontologie, Monatshefte 7:385–390.

Buffetaut, E., H. Tong, V. Suteethorn, and L. Raksaskulwong. 1994c. Jurassic vertebrates from the southern Peninsula of Thailand and their implications, a preliminary report. Proceedings of the International Symposium on Stratigraphic Correlation of Southeast Asia. 15-20 November. Bangkok, Thailand. 253-256.

Buffetaut, E., S. Suteethorn, V. Suteethorn, U. Deesri, and H. Tong. 2014. Preliminary note on a small ornithopod dinosaur from the Phu Kradung Formation (terminal Jurassic–basal Cretaceous) of Phu Noi, north-eastern Thailand. Journal of Science and Technology Mahasarakham University 33:344–347.

Buffetaut, E., V. Suteethorn, S. Suteethorn, U. Deesri, and H. Tong. 2015. An azhdarchoid pterosaur humerus from the latest Jurassic (Phu Kradung Formation) of Phu Noi, north-eastern Thailand. Research and Knowledge 1:43-47.

Carter, A., and Bristow, C. S. 2003. Linking hinterland evolution and continental basin sedimentation by using detrital zircon thermochronology: a study of the Khorat Plateau Basin, eastern Thailand. Basin Research 15:271–285.

Chanthasit, P. 2011. New theropod remains from the Phu Kradung Formation of Kalasin Province and a review of Late Jurassic theropod record in Thailand. In World Conference on Paleontology and Stratigraphy, Nakhon Rachasima, Nakhon Rachasima Rajabhat University, p. 34.

Charrière, A., F. Dépêche, M. Feist, N. Grambast-Fessard, M. Jaffrezo, B. Peybernès, and M. Ramalho. 1994. Microfaunes, microflores et paléoenvironnements successifs dans la formation d'El Mers (Bathonien-?Callovien) du synclinal de Skoura (Moyen-Atlas, Maroc). Geobios 27:157–174.

Clark, J. M. 1994. Patterns of evolution in Mesozoic Crocodyliformes; pp. 84–97 in N.C. Fraser and H-D. Sues (eds.), In the Shadow of the Dinosaurs: Early Mesozoic Tetrapods.

Cambridge University Press, Cambridge and New York.

Cornée, J. J., and Buffetaut, E. 1979. Découverte d'un Téléosauridé (Crocodylia Mesosuchia) dans le Valanginien supérieur du massif d'Allauch (sud-est de la France). Comptes Rendus de l'Académie des Sciences, Paris 288:1151–1154.

Cuny, G., P. Srisuk, P. Khama, V. Suteethorn, and H. Tong. 2009. A new elasmobranch fauna from the Middle Jurassic of southern Thailand; pp. 97–113 in E. Buffetaut, G. Cuny, J. Le Loeuff, and V. Suteethorn (eds.), Late Palaeozoic and Mesozoic Ecosystems in SE Asia. Volume Special Publications 315, Geological Society, London.

Cuny, G., A. M. Cobbett, F. J. Meunier, and M. J. Benton. 2010. Vertebrate microremains from the Early Cretaceous of southern Tunisia. Geobios 43:615–628.

Cuny, G., R. Liard, U. Deesri, T. Liard, S. Khamha, and V. Suteethorn. 2014. Shark faunas from the Late Jurassic—Early Cretaceous of northeastern Thailand. Paläontologische Zeitschrift 88:309–328.

Currie, P. J., and Zhao, X. J. 1993. A new carnosaur (Dinosauria, Theropoda) from the Jurassic of Xinjiang, People's Republic of China. Canadian Journal of Earth Sciences 30:2037–2081.

Danilov, I. G., and Parham, J. F. 2007. The type series of "*Sinemys*" *wuerhoensis*, a problematic turtle from the Lower Cretaceous of China, includes at least three taxa. Palaeontology 50:431–444.

Deesri, U., K. Lauprasert, V. Suteethorn, K. Wongo, and L. Cavin. 2014. A new ginglymodian fish (Actinopterygii, Holostei) from the Late Jurasic Phu Kradung Formation, northeastern Thailand. Acta Palaeontologica Polonica 59:313–331.

Deesri, U., Jintasakul, P., and Cavin, L. 2016. A new Ginglymodi (Actinopterygii, Holostei) from the Late Jurassic–Early Cretaceous of Thailand, with comments on the early diversification of Lepisosteiformes in Southeast Asia. Journal of Vertebrate Paleontology

36:e1225747.

Dong, Z. 1973. Dinosaurs from Wuerho. Institute of Vertebrate Paleontology and Paleoanthropology, Memoir 11:45–52. [In Chinese]

Dong, Z. 1984. A new prosauropod from Ziliujing Formation of Sichuan Basin. Vertebrata Palasiatica 22:310–313. [In Chinese]

Dong Z., Y. Zhang, X, Li, and S. Zhou. 1978. Note on a new carnosaur *Yuangchuanosaurus shangyuensis* gen. et sp. nov. from the Jurassic of Yuangchuan District, Sichuan Province. Kexue Tongbao 23:298–302. [In Chinese]

Dong Z., S. Zhou, and Y. Zhang. 1983. The dinosaurian remains from Sichuan Basin, China. Palaeontologia Sinica, N.S. 23:1–145.

Eberth, D. A. 2015. Origins of dinosaur bonebeds in the Cretaceous of Alberta, Canada. Canadian Journal of Earth Sciences 52:655–681.

Efimov, M. B. 1982. New fossil crocodiles from the USSR. Paleontological Journal 16:140–145.

Efimov, M. B. 1988. The fossil crocodiles and champsosaurides of mongolia and USSR. Transactions of the joint Soviet-Mongolian paleontological expedition 36:1–108. [In Russian]

Efimov, M. B., and V. M. Chkhikvadze. 1987. Survey of the finds of fossil crocodiles in the USSR. Izvestiya Akademii Nauk Gruzinskoi SSR, Seriya Biologicheskaya 13:200–207. [In Russian]

Eudes-Deslongchamps, J. A. 1863–1867. Notes Paléontologiques, Volume 1, Le Blanc-Hardel, Caen, Savy, Paris 392 pp.

Eudes-Deslongchamps, J. A. 1870. Notes sur les reptiles fossiles appartenant à la famille des téléosauriens, dont les débris ont été recueillis dans les assises jurassiques de la Normandie. Bulletin de la Société Géologique de France 20:299–349.

Fanti, F., Miyashita, T., Cantelli, L., Mnasri, F., Dridi, J., Contessi, M., and A. Cau. 2016. The largest thalattosuchian (Crocodylomorpha) supports teleosaurid survival across the Jurassic-Cretaceous boundary. Cretaceous Research 61:263–274.

Fernández, M., and Z. Gasparini. 2008. Salt glands in the Jurassic metriorhynchid *Geosaurus*: implications for the evolution of osmoregulation in Mesozoic marine crocodyliforms. Naturwissenschaften 95:79–84.

Fernández, M. S., A. P. Carabajal, Z. Gasparini, and G. Chong Diaz. 2011. A metriorhynchid crocodyliform braincase from northern Chile. Journal of Vertebrate Paleontology 31:369–377.

Fraas, E. V. 1901. Die Meerkrokodile (Thalattosuchia n.g.) eine Sauriergruppe der Juraformation. Jahresheft der Vereinigung vaterländischer Naturkundler Württembergs 57:409–418.

Gasparini, Z. B., P. Vignaud, and G. Chong. 2000. The Jurassic Thalattosuchia (Crocodyliformes) of Chile : a paleobiogeographic approach. Bulletin de la Société Géologique de France 171:657–664.

Geoffroy Saint-Hilaire, E. 1825. Recherches sur l'organisation des Gavials, sur leurs affinités naturelles desquelles résulte la necessité d'une autre distribution générique: *Gavialis*, *Teleosaurus*, *Steneosaurus*. Mémoires du Muséum National d'Histoire Naturelle 12:97–155.

Godefroit, P., P. Vignaud, and A. Lieger. 1995. Un Teleosauridae (Reptilia) du Bathonien Supérieur Lorrain (France). Bulletin de la Société Belge de Géologie 104:91–107.

Goloboff, P. A., J. S. Farris, and K. C. Nixon. 2008. TNT, a free program for phylogenetic analysis. Cladistics 24:774–786.

Hay, O. P. 1930. Second bibliography and Catalogue of the Fossil Vertebrata of North America, Volume II. Carnegie Institution of Washington Publication No. 390.

Washington D.C.

Herrera, Y., M., M. S. Fernández, and Z. Gasparini. 2013. The snout of *Cricosaurus araucanensis*: a case study in novel anatomy of the nasal region of metriorhynchids. Lethaia 46:331–340.

Herrera, Y., Z. Gasparini, and M. S. Fernández. 2015. *Purranisaurus potens* Rusconi, an enigmatic metriorhynchid from the Late Jurassic–Early Cretaceous of the Neuquén Basin. Journal of Vertebrate Paleontology 35:e904790.

Hirayama, R. 2006. Review of fossil turtles of Japan. Fossils 80:47–59.

Holliday, C. S., and L. M. Witmer. 2009. The epipterygoid of crocodyliforms and its significance for the evolution of the orbitotemporal region of eusuchians. Journal of Vertebrate Paleontology 29:715–733.

Hua, S., and V. de Buffrénil. 1996. Bone histology as a clue in the interpretation of functional adaptations in the Thalattosuchia (Reptilia, Crocodylia). Journal of Vertebrate Paleontology 16:703–717.

Irmis, R. B. 2007. Axial skeleton ontogeny in the Parasuchia (Archosauria : Pseudosuchia) and its implications for ontogenetic determination in archosaurs. Journal of Vertebrate Paleontology 27:350–361.

Johnson, M. M., M. T. Young, L. Steel, D. Foffa, A. S. Smith, S. Hua, P. Havlik, E. A. Howlett, and G. Dyke. 2017. Re-description of '*Steneosaurus*' *obtusidens* Andrews, 1909, an unusual macrophagous teleosaurid crocodylomorph from the Middle Jurassic of England. Zoological Journal of the Linnean Society 182:385–418.

Jouve, S. 2009. The skull of *Teleosaurus cadomensis* (Crocodylomorpha: Thalattosuchia), and phylogenetic analysis of Thalattosuchia. Journal of Vertebrate Paleontology 29:88–102.

Klug, S., T. Tütken, O. Wings, H.-U. Pfretzschner, and T. Martin. 2010. A Late Jurassic

freshwater shark assemblage (Chondrichthyes, Hybodontiformes) from the southern Junggar Basin, Xinjiang, Northwest China. Palaeobiodiversity and Palaeoenvironments 90:241–257.

Kofron, C. P. 1993. Behavior of Nile crocodiles in a seasonal river in Zimbabwe. Copeia 1993:463–469.

Krebs, B. 1967. Der Jura-Krokodilier *Machimosaurus* H. v. Meyer. Palaeontologische Zeitschrift 41:46–49.

Krebs, B. 1968. Le crocodilien *Machimosaurus*. Contribuçao para o conhecimento da fauna do Kimeridgiano da mina de lignito Guimarota (Leira, Portugal), 1. Memorias do Serviços Geologicos de Portugal 14:1–53.

Krymholts, G. Y., and Mesezhnikov, M.S. 1988. The Jurassic ammonite zones of the Soviet Union. Geological Society of America Special Papers 223:10.1130/SPE223-p1

Lapparent, A.F. 1955. Etude paléontologique des vertébrés du Jurassique d'El Mers (Moyen Atlas). Editions du service géologique du Maroc, Rabat, Notes et Mémoires 124:7–36.

Lauprasert, K., G. Cuny, E. Buffetaut, V. Suteethorn, and K. Thirakhupt. 2007. *Siamosuchus phuphokensis*, a new goniopholidid from the Early Cretaceous (ante-Aptian) of northeastern Thailand. Bulletin de la Société Géologique de France 178:201–216.

Li, J. 1993. A new specimen of *Peipehsuchus teleorhinus* from Ziliujing Formation of Daxian, Sichuan. Vertebrata Palasiatica 31:85–94.

Liard, R., and J.E. Martin. 2011. Relative position of the Mesozoic vertebrate localities in the Phu Kradung Formation of the Phu Phan uplift, Northeast Thailand [abstract]; pp. 191–192 in World Conference on Paleontology and Stratigraphy (WCPS2011). Nakhorn Ratchasima, Thailand, 28 November 2011–2 December 2011, Abstract. Nakhon Ratchasima Rajabhat University.

Liard, R., G. Cuny, J. Martin, T. Liard, U. Deesri, and S. Suteethorn. 2015. Phu Noi, a

mesozoic vertebrate locality from the Jurassic of Thailand. 5th GEOINDO, International Conference on Geology, Geotechnology, and Mineral Resources of Indochina. 23-24 November 2015, Centara Hotel and Convention Centre, Khon Kaen, Thailand.

Maisch, M. W., and A. T. Matzke. 2005. Temnospondyl amphibians from the Jurassic of the Southern Junggar Basin (NW China). Paläontologische Zeitschrift 79:285–301.

Martin, J. E., R. Amiot, C. Lécuyer, and M. J. Benton. 2014a. Sea surface temperature contributes to marine crocodylomorph evolution. Nature Communications 5:4658, doi:10.1038/ncomms5658.

Martin, J. E., Lauprasert, K., Buffetaut, E., Liard, R., and Suteethorn, V. 2014b. A large pholidosaurid in the Phu Kradung Formation of northeastern Thailand. Palaeontology 57:757–769.

Martin, J. E., and P. Vincent. 2013. New remains of *Machimosaurus hugii* von Meyer, 1837 (Crocodilia, Thalattosuchia) from the Kimmeridgian of Germany. Fossil Record, 16:179–196.

Martin, J. E., Vincent, P., and Falconnet, J. 2015. The taxonomic content of *Machimosaurus* (Crocodylomorpha, Thalattosuchia). Comptes Rendus Palevol 14 :305–310.

Martin, J. E., U. Deesri, R. Liard, A. Wattanapituksakul, S. Suteethorn, K. Lauprasert, H. Tong, E. Buffetaut, V. Suteethorn, G. Suan, P. Telouk, and V. Balter. 2016. Strontium isotopes reveal long-term residence of thalattosuchians in the freshwater environment. Paleobiology 42:142–156.

McPhee, B. W., P. Upchurch, P. D. Mannion, C. Sullivan, R. J. Butler., and P. M. Barrett. 2016. A revision of *Sanpasaurus yaoi* Young, 1944 from the Early Jurassic of China, and its relevance to the early evolution of Sauropoda (Dinosauria). PeerJ 4 :e2578.

Morel de Glasville, M. 1876. Sur la cavité crânienne et la position du trou optique dans le *Steneosaurus heberti*. Bulletin de la Société Géologique de France 3(4):342–348.

Mueller-Töwe, I. J. 2005. Phylogenetic relationships of the Thalattosuchia. Zitteliana 45:211–213.

Mueller-Töwe, I. J. 2006. Anatomy, phylogeny, and palaeoecology of the basal thalattosuchians (Mesoeucrocodylia) from the Liassic of Central Europe. PhD Thesis, Mainz, 422 pp.

Newton, R. B. 1893. On the discovery of a secondary reptile in Madagascar: *Steneosaurus baroni* (n. sp.); with a reference to some post-tertiary vertebrate remains from the same country recently acquired by the British Museum (Natural History). Geological Magazine 10:193–198.

Peng, G. -Z., Y. Ye, Y.-H. Gao, C. -K. Shu, and S. Jiang. 2005. Jurassic Dinosaur Faunas in Zigong. People's Publishing House of Sichuan, Chengdu, China, 236 pp.

Pérez-García, A., F. R. Sáez-Benito, and X. Murelaga. 2017. New information on the anatomy and systematics of the Spanish Lower Cretaceous *Camerochelys vilanovai* (Testudines, Pan-Cryptodira). Journal of Iberian Geology 43:147–154.

Pierce, S. E., and M. J. Benton. 2006. *Pelagosaurus typus* Bronn, 1841 (Mesoeucrocodylia: Thalattosuchia) from the Upper Lias (Toarcian, Lower Jurassic) of Somerset, England. Journal of Vertebrate Paleontology, 26:621–635.

Pierce, S. E., K. D. Angielczyk, and E. J. Rayfield. 2009. Morphospace occupation in thalattosuchian crocodylomorphs: skull shape variation, species delineation and temporal patterns. Palaeontology 52:1057–1097.

Pierce, S. E., M. Williams, and R. B. Benson. 2017. Virtual reconstruction of the endocranial anatomy of the early Jurassic marine crocodylomorph *Pelagosaurus typus* (Thalattosuchia). PeerJ 5:e3225.

Racey, A., and J. G. Goodall. 2009. Palynology and stratigraphy of the Mesozoic Khorat Group red bed sequences from Thailand. Geological Society, London, Special Publications 315:69–83.

Rees, J., and C.J. Underwood. 2008. Hybodont sharks of the English Bathonian and Callovian (middle Jurassic). Palaeontology 51, 117–147.

Rees, J., and C. J. Underwood. 2006. Hybodont sharks from the Middle Jurassic of the Inner Hebrides, Scotland. Transactions of the Royal Society of Edinburgh: Earth Sciences 96, 351–363.

Storrs, G. W., and M. B. Efimov. 2000. Mesozoic crocodyliforms of north-central Eurasia. In Benton, M. J., Shishkin, M. A., Unwin, D. M., and Kurochkin, E. N. The Age of Dinosaurs in Russia and Mongolia, 402–419.

Suteethorn, V., J. Le Loeuff, E. Buffetaut, V. Suteethorn, and K. Wongko. 2013. First evidence of a mamenchisaurid dinosaur from the Upper Jurassic–Lower Cretaceous Phu Kradung Formation of Thailand. Acta Palaeontologica Polonica 58:459–469.

Syme, C. E., and S. W. Salisbury. 2014. Patterns of aquatic decay and disarticulation in juvenile Indo-Pacific crocodiles (*Crocodylus porosus*), and implications for the taphonomic interpretation of fossil crocodyliform material. Palaeogeography, Palaeoclimatology, Palaeoecology 412:108–123.

Tennant, J. P., P. D., Mannion, P. Upchurch, M. D. Sutton, and G. D. Price. 2017. Biotic and environmental dynamics through the Late Jurassic–Early Cretaceous transition: evidence for protracted faunal and ecological turnover. Biological Reviews 92:776–814.

Timm, R. M. 1982. Dermestids. Field Museum of Natural History Bulletin 53:14–18.

Tong, H., J. Claude, W. Naksri, V. Suteethorn, E. Buffetaut, S. Khansubha, W. Wongko, and P. Yuangdetkla. 2009. *Basilochelys macrobios* n. gen. and n. sp., a large cryptodiran

turtle from the Phu Kradung Formation (latest Jurassic-earliest Cretaceous) of the Khorat Plateau, NE Thailand. Geological Society, London, Special Publications 315:153–173.

Tong, H., W. Naksri, E. Buffetaut, V. Suteethorn, S. Suteethorn, U. Deesri, S. Sila, P. Chanthasit, and J. Claude. 2015. A new primitive eucryptodiran turtle from the Upper Jurassic Phu Kradung Formation of the Khorat Plateau, NE Thailand. Geological Magazine 152:166–175.

Warren, A., and C. Marsicano. 2003. A phylogeny of the Brachyopoidea (Temnospondyli, Stereospondyli). Journal of Vertebrate Paleontology 20:462–483.

Westphal, F. 1961. Zur Systematik der deutschen und englischen Lias-Krokodilier. Neues Jahrbuch für Geologie und Paläontologie Abhandlungen 113:207–218.

Westphal, F. 1962. Die krokodilier des Deutschen und Englischen oberen Lias. Palaeontographica A 116:23–118.

Wilberg, E. W. 2015a. A new metriorhynchoid (Crocodylomorpha, Thalattosuchia) from the Middle Jurassic of Oregon and the evolutionary timing of marine adaptations in thalattosuchian crocodylomorphs. Journal of Vertebrate Paleontology 35:e902846.

Wilberg, E. W. 2015b. What's in an outgroup? The impact of outgroup choice on the phylogenetic position of Thalattosuchia (Crocodylomorpha) and the origin of Crocodyliformes. Systematic Biology 64:621–637.

Xing, L., T. Miyashita, J. Zhang, D. Li, Y. Ye, T. Sekiya, F. Wang, and P. J. Currie. 2015. A new sauropod dinosaur from the Late Jurassic of China and the diversity, distribution, and relationships of mamenchisaurids. Journal of Vertebrate Paleontology 35:e889701.

Young, C. C. 1948. Fossil crocodiles in China, with notes on dinosaurian remains associated with the Kansu crocodiles. Vertebrata Palasiatica 28:255–288.

Young, M. T., and M. B. Andrade. 2009. What is *Geosaurus* ? Redescription of *Geosaurus giganteus* (Thalattosuchia : Metriorhynchidae) from the Upper Jurassic of Bayern,

Germany. Zoological Journal of the Linnean Society 157:551–585.

Young, M. T., S. L. Brusatte, M. B. Andrade, J. B. Desojo, B. L. Beatty, L. Steel, M. S. Fernández, M. Sakamoto, J. Ruiz-Omeñaca, and R. Schoch. 2012. The cranial osteology and feeding ecology of the metriorhynchid crocodylomorph genera *Dakosaurus* and *Plesiosuchus* from the Late Jurassic of Europe. PLoS One 7:e44985.

Young, M. T., M. B. Andrade, J.-J. Cornée, L. Steel, and D. Foffa. 2014. Re-description of a putative Early Cretaceous "teleosaurid" from France, with implications for the survival of metriorhynchids and teleosaurids across the Jurassic-Cretaceous boundary. Annales de Paléontologie 100:165–174.

Submitted January 8, 2018; accepted Month DD, YYYY

Figure Captions

FIGURE 1. Overview of the specimens of *Indosinosuchus potamosiamensis* gen. et sp. nov. represented by cranial material discovered since 2008 at the Phu Noi locality and illustrating size variability in this small population of teleosaurids. **A**, dentary of juvenile KS34-1213; **B**, PRC-8; **C**, PRC-9; **D**, PRC-10; **E**, PRC-238; **F**, PRC-11; **G**, KS33-209; **H**, PRC-12; **I**, PRC-239; **J**, PRC-240. Scale bar equals 20 cm. [planned for full page width]

FIGURE 2. Photographs of the holotype (PRC-11) skull and mandibles of *Indosinosuchus potamosiamensis* gen. et sp. nov. from the Phu Kradung Formation of Phu Noi, northeastern Thailand in **A**, dorsal; **B**, ventral and **C**, lateral views. [planned for full page width]

FIGURE 3. Line drawings of the holotype (PRC-11) skull and mandibles of *Indosinosuchus potamosiamensis* gen. et sp. nov. from the Phu Kradung Formation of Phu Noi, northeastern

Thailand in **A**, dorsal; **B**, ventral and **C**, lateral views. **Abbreviations**: **an**, angular; **aof**, antorbital fenestra; **art**, articular; **boc**, basioccipital; **bsph**, basisphenoid; **ch**, choanae; **co**, coronoid; **den**, dentary; **en**, external nares; **emf**, external mandibular fenestra; **ec**, ectopterygoid; **exo**, exoccipital; **fo**, foramen; **fr**, frontal; **gr**, groove; **j**, jugal; **jd**, jugal depression; **l**, lacrimal; **ltsph**, laterosphenoid; **mx**, maxilla; **n**, nasal; **on,** otic notch; **otf,** orbitotemporal foramen; **p**, parietal; **pal**, palatine; **pf**, palatine foramina; **pfr**, prefrontal; **pmx**, premaxilla; **po**, postorbital; **pt**, pterygoid; **q**, quadrate; **qj**, quadratojugal; **san**, surangular; **sp**, splenial; **sq**, squamosal; **sqs**, squamosal flat surface; **1–27**, alveolar count; **V,** trigeminal opening for the fifth cranial nerve. [planned for full page width]

FIGURE 4. Close-up of the premaxillae of the holotype specimen (PRC-11) of *Indosinosuchus potamosiamensis* gen. et sp. nov. from the Phu Kradung Formation of Phu Noi, northeastern Thailand. **A**, dorsal view; **B**, left lateral view; **C**, ventral view. **Abbreviations**: **den**, dentary; **en**, external nares; **if**, incisive foramen; **pms**, premaxillary-maxillary suture; **pp**, premaxillary process; **1–4**, premaxillary alveolar count. [planned for column width]

FIGURE 5. Premaxillary and maxillary alveolar reconstructions from CT data from the holotype specimen (PRC-11) of *Indosinosuchus potamosiamensis* gen. et sp. nov. from the Phu Kradung Formation of Phu Noi, northeastern Thailand. **A**, general view of the reconstructed transparent skull and mandible; **B**, detailed of the reconstructed premaxillary and maxillary alveolar rows. Green color corresponds to filled alveolar space and blue color corresponds to replacement dentition. **Abbreviations**: **mx**, maxilla; **pmx**, premaxilla. [planned for full page width]

FIGURE 6. Anatomical details of the holotype specimen (PRC-11) of *Indosinosuchus potamosiamensis* gen. et sp. nov. from the Phu Kradung Formation of Phu Noi, northeastern Thailand. **A**, oblique dorsolateral view of the right supratemporal fossa; **B**, right anterolateral view of the antorbital area; **C**, right lateral view of the otic area; **D**, left anterolateral view of the antorbital area. **Abbreviations**: **aof**, antorbital fenestra; **cdq**, circular depression on quadrate; **exo**, exoccipital; **fr**, frontal; **j**, jugal; **l**, lacrimal; **ltf**, lower temporal fenestra; **ltsph**, laterosphenoid; **mx**, maxilla; **n**, nasal; **on**, otic notch; **or**, orbit; **p**, parietal; **po**, postorbital; **pro**, prootic; **q**, quadrate; **qj**, quadratojugal; **sq**, squamosal; **sqs**, squamosal flat surface; **stf**, supratemporal fenestra; **V**, exit for cranial nerve V. [planned for full page width]

FIGURE 7. Photographs and line drawings of specimen PRC-12 of *Indosinosuchus potamosiamensis* gen. et sp. nov. including skull, mandibles and disarticulated postcranial elements recovered from the Phu Kradung Formation of Phu Noi, northeastern Thailand; **A**, **B**, dorsal and **C**, **D**, ventral views. **Abbreviations**: **an**, angular; **aof**, antorbital fenestra; **art**, articular; **boc**, basioccipital; **bsph**, basisphenoid; **ch**, choanae; **cr**, cervical rib; **cv**, cervical vertebra; **den**, dentary; **dv**, dorsal vertebra; **en**, external nares; **emf**, external mandibular fenestra; **ec**, ectopterygoid; **fr**, frontal; **j**, jugal; **l**, lacrimal; **mmf**, medial mandibular fenestra; **mx**, maxilla; **n**, nasal; **oc**, occipital condyle; **ost**, osteoderm; **p**, parietal; **pal**, palatine; **pf**, palatal foramina; **pfr**, prefrontal; **pmx**, premaxilla; **po**, postorbital; **pt**, pterygoid; **q**, quadrate; **r**, rib; **san**, surangular; **sof**; suborbital fenestra; **sp**, splenial; **sq**, squamosal; **sqs**, squamosal concave surface; **1–4**, premaxillary alveolar count. [planned for 2/3 page width]

FIGURE 8. **A**, Photographs and **B**, line drawings of specimen PRC-238 of *Indosinosuchus potamosiamensis* gen. et sp. nov. from the Phu Kradung Formation of Phu Noi, northeastern

Thailand in dorsal view. **Abbreviations**: **an**, angular; **aof**, antorbital fenestra; **art**, articular; **boc**, basioccipital; **bsph**, basisphenoid; **ec**, ectopterygoid; **en**, external nares; **fr**, frontal; **j**, jugal; **l**, lacrimal; **n**, nasal; **pmx**, premaxilla; **pre**, prearticular; **pfr**, prefrontal; **po**, postorbital; **pt**, pterygoid; **sof**, suborbital fenestra; **sp**, splenial. [planned for column width]

FIGURE 9. **A**, Photographs and **B**, line drawings of specimen PRC-238 of *Indosinosuchus potamosiamensis* gen. et sp. nov. from the Phu Kradung Formation of Phu Noi, northeastern Thailand in ventral view. **Abbreviations**: **an**, angular; **boc**, basioccipital; **bsph**, basisphenoid; **ch**, choana; **den**, dentary; **ec**, ectopterygoid; **emf**, external mandibular fenestra; **pal**, palatine; **pt**, pterygoid; **sof**, suborbital fenestra; **sp**, splenial. [planned for column width]

FIGURE 10. Photographs of the partial skull dorsum of *Indosinosuchus potamosiamensis* gen. et sp. nov. (PRC-8) from the Phu Kradung Formation of Phu Noi, Thailand and associated line drawings in **A** and **B**, dorsal; **C** and **D**, ventral, **E** and **F**, occipital, **G** and **H**, right lateral views. Silicon rubber endocast of the same specimen in lateral view with **I**, photograph and **J**, superimposed drawing. Scale bars equal 2 cm. **Abbreviations**: **boc**, basioccipital; **bsph**, basisphenoid; **cB**, crest B of Iordansky (1973); **cb**, cerebrum; **cbl**, cerebellum; **ch**, choana; **dls**, dorsal branch of longitudinal sinus; **ec**, ectopterygoid; **exo**, exoccipital; **fcp**, foramen caroticum posterius; **fm**, foramen magnum; **fr**, frontal; **fv**, foramen vagi; **j**, jugal; **leu**, lateral Eustachian opening; **ltsp**, laterosphenoid; **mo**, medulla oblonga; **oc**, occipital condyle; **on**, otic notch; **ot**, olfactory tract; **otf**, orbitotemporal fenestra; **or**, orbit; **p**, parietal; **?pi**, pituitary; **po**, postorbital; **pro**, prootic; **pt**, pterygoid; **ptf**, posttemporal foramen; **q**, quadrate; **soc**, supraoccipital; **sof**, suborbital fenestra; **sq**, squamosal; **sqs**, squamosal flat surface; **stf**, supratemporal fenestra; **tbi**, tympanic bulla imprint; **tt**, torus transiliens; **tub**, basioccipital tuberosity; **V**, exit for cranial nerve V; **XII**, exit for cranial nerve XII; arrows

indicate a pair of muscle scars on the dorsal edge of the squamosal. [planned for full page width]

FIGURE 11. Detailed tooth morphology of *Indosinosuchus potamosiamensis* gen. et sp. nov. from the Phu Kradung Formation of Phu Noi. **A**, general aspect of the crown in mesiolabial view (PRC-13 belonging to PRC-239); **B**, cross section in the apical region (PRC-14 belonging to PRC-11) and **C**, detail of the cross section. * indicate the mesiodistal carinae of the enamel and the arrow indicates the shape of the carina at the enamel-dentine junction. [planned for column width]

FIGURE 12. The postcranial skeleton of *Indosinosuchus potamosiamensis* gen. et sp. nov. from the Phu Kradung Formation of Phu Noi. Atlas (PRC-15) in **A**, anterior and **B**, ventral views; atlas-axis complex (PRC-17) in **C**, left lateral and **D**, ventral views; cervical vertebra (PRC-18) in **E**, right lateral and **F**, ventral views; left cervical rib (PRC-19) in **G**, posterior and **H**, medial views; thoracic vertebrae (PRC-20 and 21) in **I**, anterior and **J**, left lateral views; **K**, PRC-22 articulated vertebral colum in left lateral view. **Abbreviations**: **ana**, axis neural arch; **ax**, axis; **c**, cervical vertebra; **t**, thoracic vertebra; **s**, sacral vertebra; **ca**, caudal vertebra. [planned for column width]

FIGURE 13. The forelimb of *Indosinosuchus potamosiamensis* gen. et sp. nov. from the Phu Kradung Formation of Phu Noi. Left humerus (PRC-23) in **A**, posterior; **B**, anterior; **C**, proximal; **D**, distal views. Right scapula (PRC-24) in **E**, lateral; **F**, medial; and **G**, proximal views. **Abbreviations**: **amer**, anteromedial epicondylar ridge; **dpc**, deltopectoral crest; **hh,** humeral head; **ler**, lateral epicondylar ridge; **scr**, supracondylar ridge. [planned for full page width]

FIGURE 14. The hind limb of *Indosinosuchus potamosiamensis* gen. et sp. nov. from the Phu Kradung Formation of Phu Noi. Left femur (PRC-25 from specimen PRC-12) in **A**, medial; **B**, lateral; **C**, proximal; **D**, distal views. Left ilium (PRC-26) in **E**, lateral and **F**, ventral views. **G**, right ischium (PRC-27) in medial view. **Abbreviations**: **acetf**, acetabular fossa; **ap**, anterior process; **lc**, lateral condyle; **mc**, medial condyle; **4t**, fourth trochanter. [planned for full page width]

FIGURE 15. The armour of *Indosinosuchus potamosiamensis* gen. et sp. nov. from the Phu Kradung Formation of Phu Noi. A, isolated element of the dorsal shield (PRC-29); B, connected elements of the ventral shield (PRC-30). **Abbreviations**: **alp**, anterolateral process; af, anterior facet. [planned for full page width]

FIGURE 16. **A**, Strict consensus of 10 most parsimonious trees recovered in this analysis indicating a phylogenetic placement of the new Thai taxon within Teleosauroidea. **B**, second consensus of a single tree obtained from the analysis of a small datamatrix, recovering a slightly different topology. [planned for full page width]

FIGURE 17. Teleosaurid specimens from the Ziliujing Formation of China. Holotype of *Peipehsuchus teleorhinus* (IVPP RV 48001) in **A**, dorsal; **B**, right lateral; **C**, ventral views. Rostrum of the specimen (IVPP RV 10098) referred to *P. teleorhinus* by Li (1993) in **D**, ventral view. [planned for column width]

FIGURE 18. **A**, Detailed view of circular rosette-type bioerosion left by a putative dermestid larva on the **B**, dorsal surface of the skull (PRC-10) of *Indosinosuchus potamosiamensis* gen.

et sp. nov. from the Late Jurassic Phu Kradung Formation of Phu Noi, **C**, as well as on the dorsal surface of the skull of the holotype specimen (PRC-11) with arrows pointing to the numerous bioerosive structures. [planned for column width]

TABLE 1. Measurement (in cm) of specimens of *Indosinosuchus potamosiamensis* gen. et sp. nov. from the Late Jurassic Phu Kradung Formation of Phu Noi.

	PRC-12	PRC-11	PRC-238	PRC-239	PRC-240	PRC-10
Length of skull (from tip of premaxilla to supraoccipital)	43	48.4	42.2	57.5	?	44
Maximal width of skull (across quadrates)	16	19	14.6	22	?	13.5
Length of snout (in front of orbits to premaxillae)	28.5	32.3	28.5	38.3	47.5	28.5
Maximal width of snout at tip of nasals	3.6	4.5	3.3	4	5	3.2
Maximal length of naris (fossa inc.)	1.5	1.8	1.7	2	3	1.7
Maximal width of naris (fossa inc.)	2.1	2.7	1.9	2.6	3.5	1.7
Diameter of orbit	3.2	4.2	3.4	4.3	5.2	3.5
Width between medial hemicondyles	10	12	?	10	?	?
Interorbital width	>2	3.5	?	3.4	6.7	2.8
Length of cranial table (through center of supratemporal fenestrae)	10.5	12.5	?	15	?	11
Width of cranial table (across centers of supratemporal fenestrae)	14	15.5	?	17	?	11.5
Maximal length of supratemporal fenestra	10.4	11.5	?	14.6	?	10

TABLE 1. (Continued)

Maximal width of supratemporal fenestra	5.7	6.3	?	6.8	8	5.5
Interfenestral width	0.3	0.5	?	0.9	?	0.4
Length of ventral border of infratemporal fenestra	?	9.5	?	11	?	?
Length of incisive foramen	?	0.4	?	?	?	?
Width of incisive foramen	?	0.2	?	?	?	?
Length of long axis of suborbital fenestra	6	5.5	5.6	8.3	10	?
Length of short axis of suborbital fenestra	2	2.6	1.5	1.7	2.5	?
Interfenestral width of palatines	3.9	4.5	3.5	3.8	6.4	2.5
Width of choanae	3	4	2.8	3	5	2
Width across basioccipital ventral surface	4.5	?	?	5	?	4.4
Occipital condyle width	2	2	?	2.7	?	1.5
Mandible length (parallel to symphysis)	54	58	47.8	68	74	?
Symphysis length	26	28.5	25.3	32.5	39	?
External mandibular fenestra length	8	8.3	5.8	10.5	12.5?	?

TABLE 1. (Continued)

External mandibular fenestra height	1.7	2	0.9	1.9	1.7	?
Glenoid fossa width	3.5	3.9	2.3	?	4	?
Retroarticular process length	6	7	5.5	8	10	?
Width at level of 13th dentary tooth	3	3.5	3	4.7	6	?


A
B
C
D
E
F
G
H
I
J
KSU-209

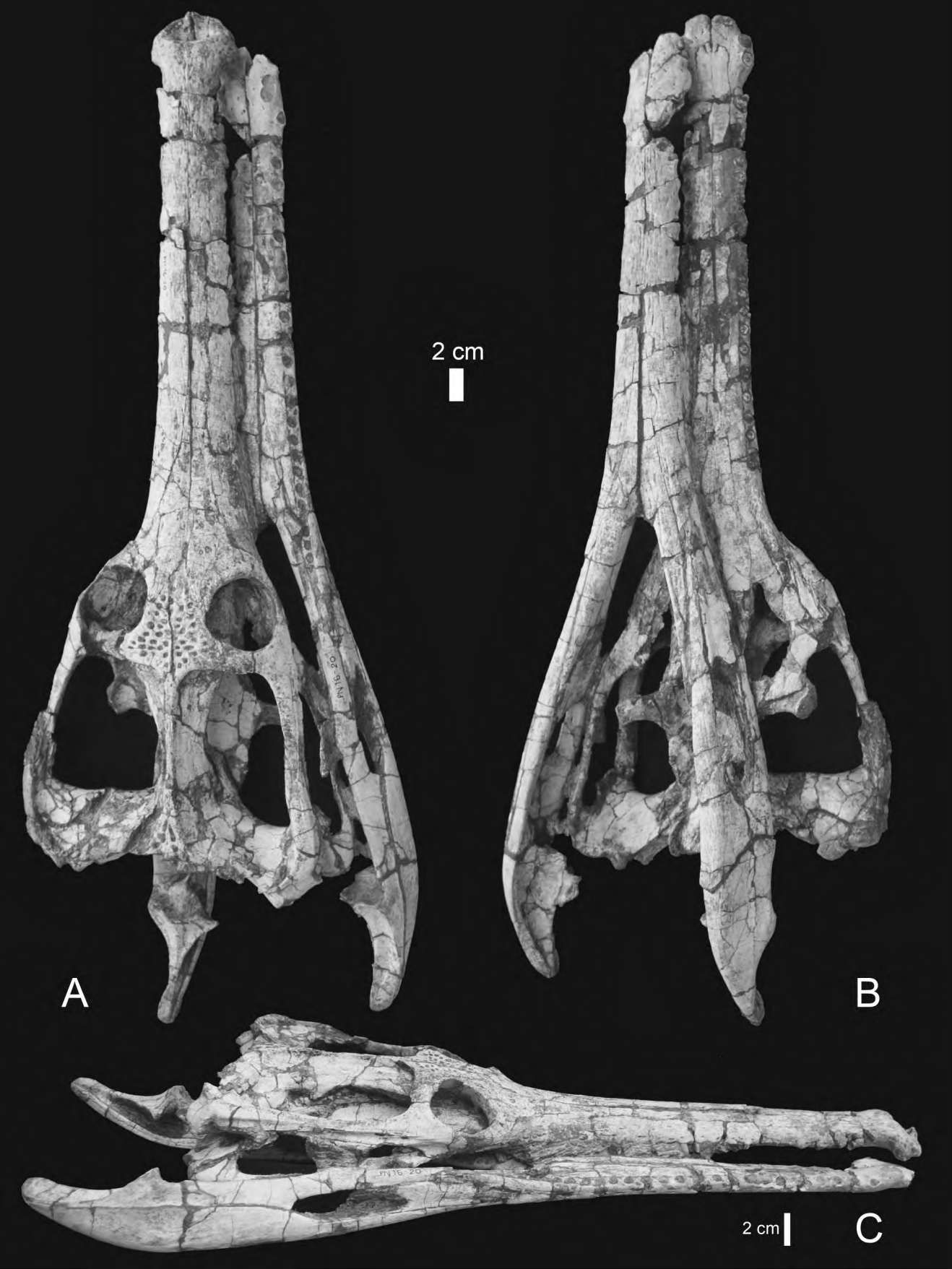
2 cm
A
B
2 cm
C

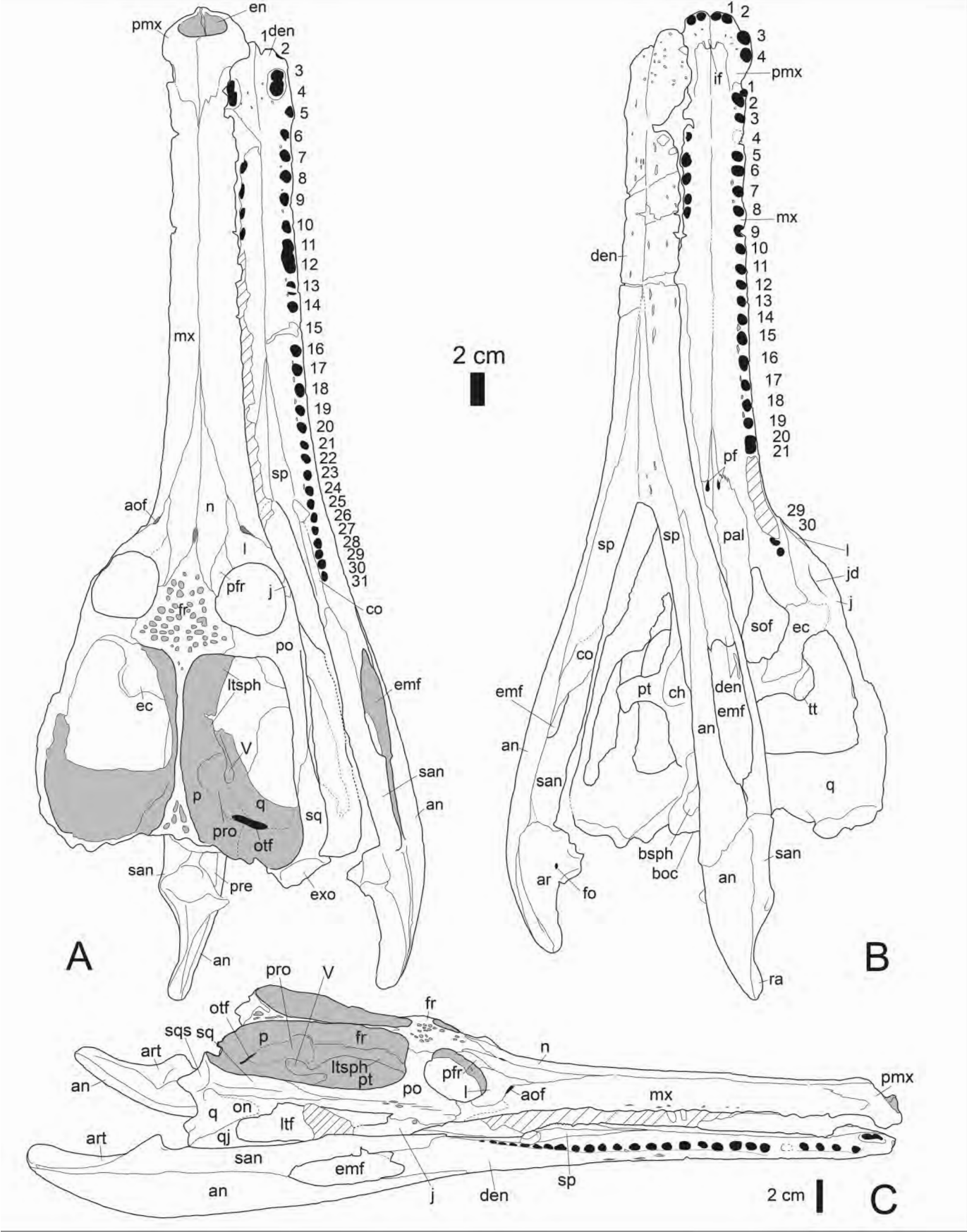
A
B
C
2 cm
2 cm
pmx
en
den
mx
sp
aof
n
l
pfr
j
fr
co
po
ltsph
emf
ec
V
san
p
q
sq
pro
otf
pre
exo
an
if
pf
pal
jd
sof
ec
tt
ch
pt
den
bsph
boc
ar
fo
ra
sqs
sq
art
on
ltf
qj
emf
fr
n
pmx
mx
aof

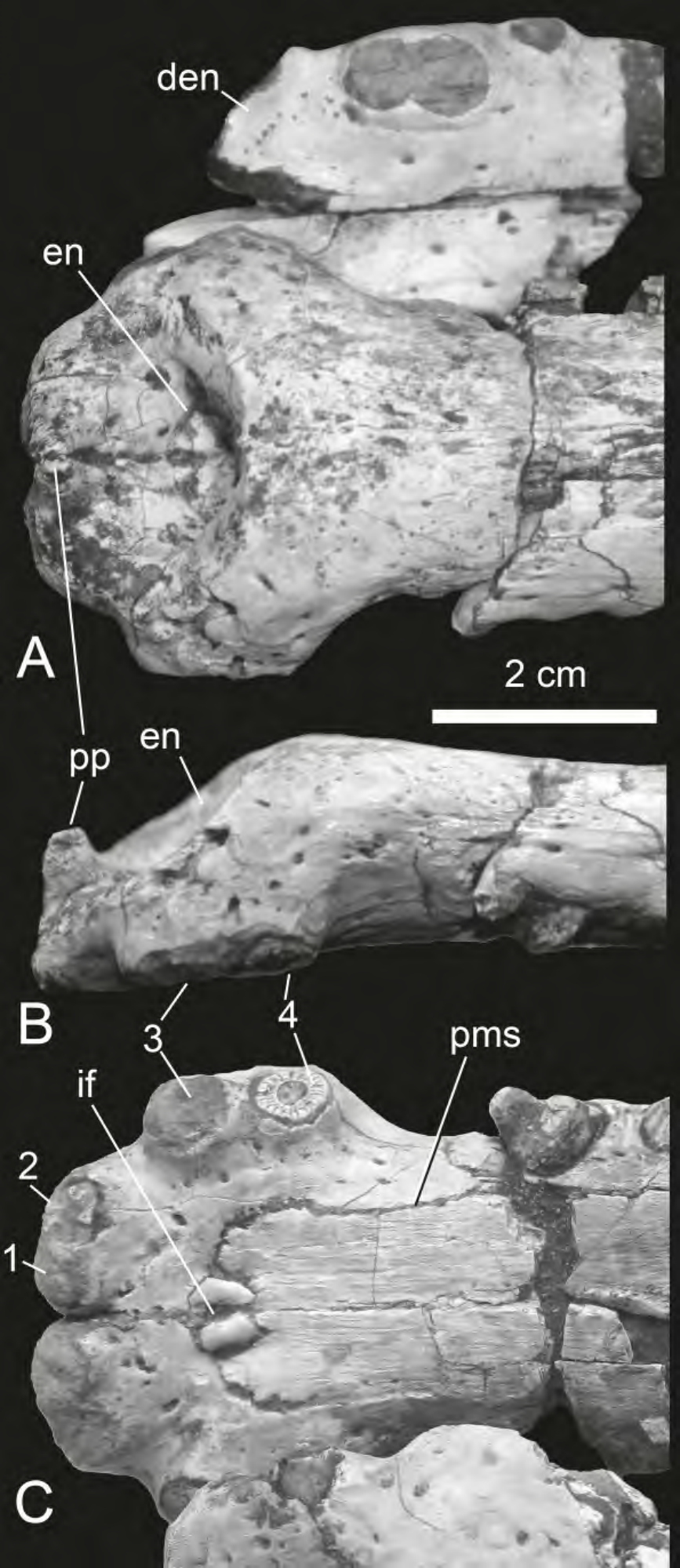
den
en
A
2 cm
pp
en
B
3
4
pms
if
2
1
C

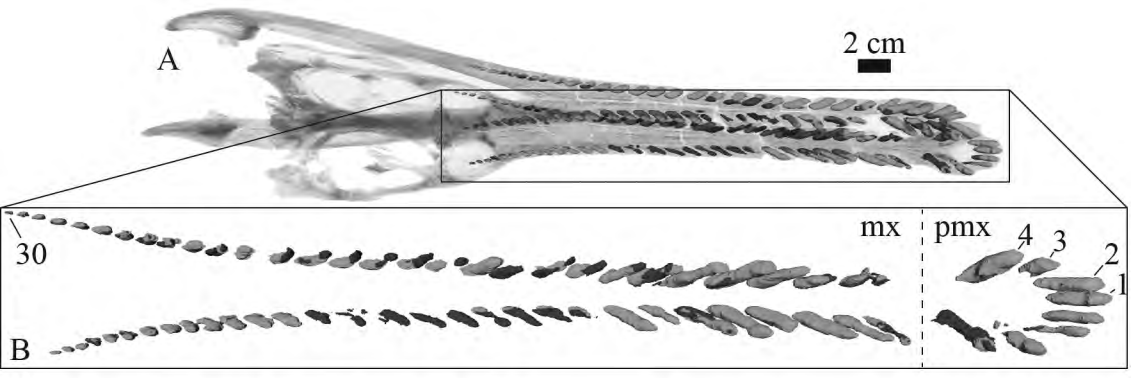
A
2 cm
30
mx
pmx
4
3
2
1
B

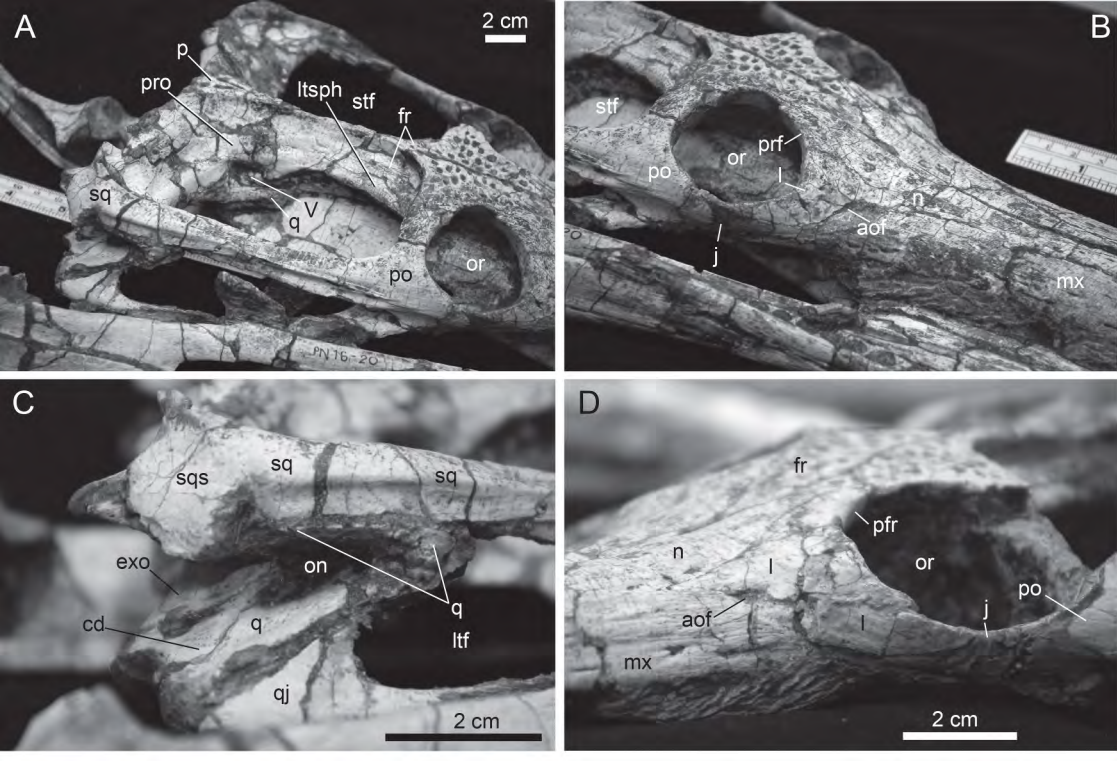
A
2 cm
p
pro
ltsph
stf
fr
sq
q
V
po
or
B
stf
prf
or
po
l
n
aof
j
mx
C
sqs
sq
sq
exo
on
q
cd
q
ltf
qj
2 cm
D
fr
pfr
n
l
or
po
aof
l
j
mx
2 cm

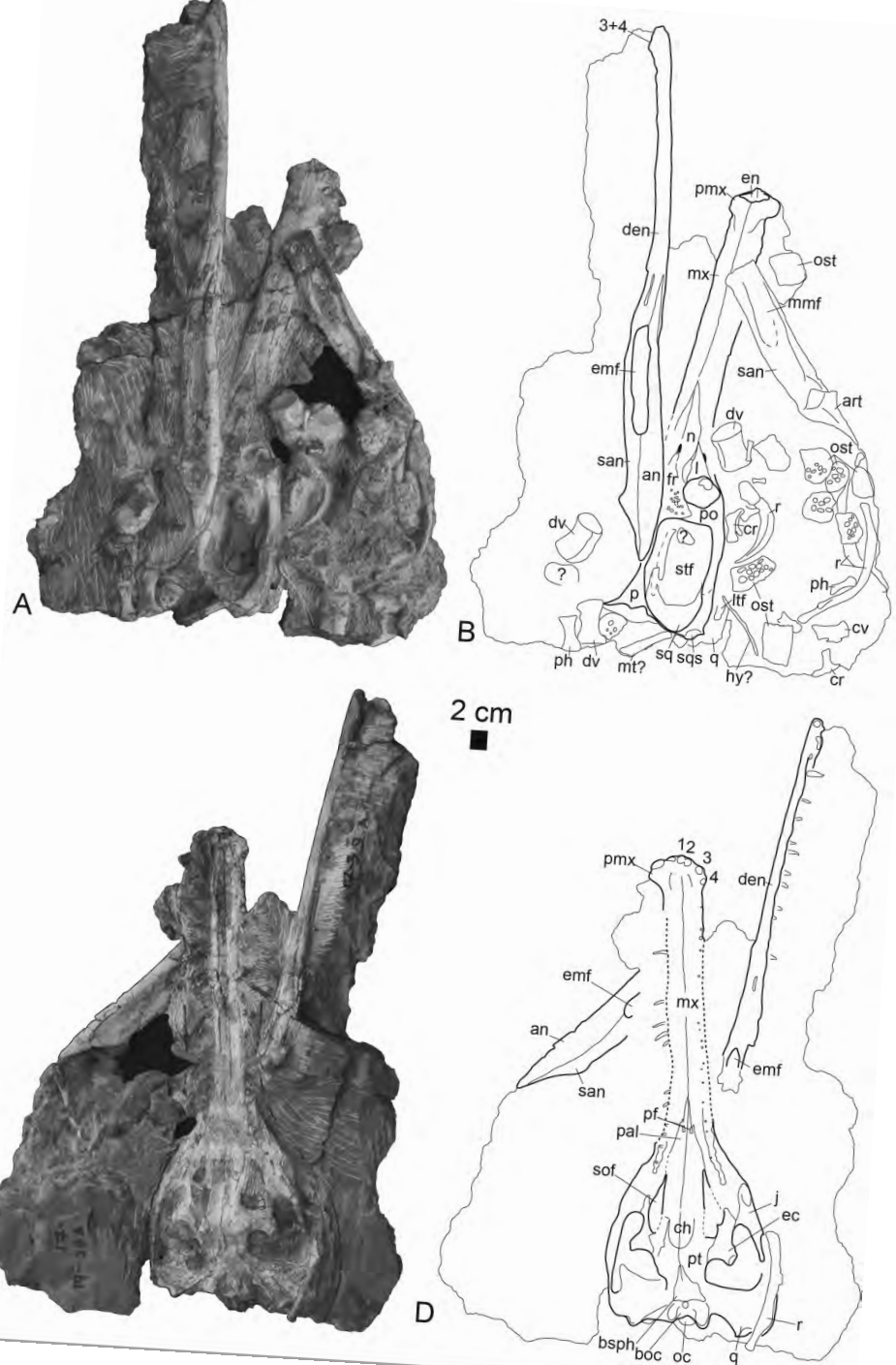
A
B
3+4
pmx
en
den
ost
mx
mmf
emf
san
art
dv
n
ost
san
an
fr
l
po
r
dv
?
cr
?
stf
r
p
ltf
ost
ph
cv
ph
dv
mt?
sq
sqs
q
hy?
cr
2 cm
D
1
2
3
4
pmx
den
emf
mx
an
emf
san
pf
pal
sof
j
ec
ch
pt
r
bsph
boc
oc
q

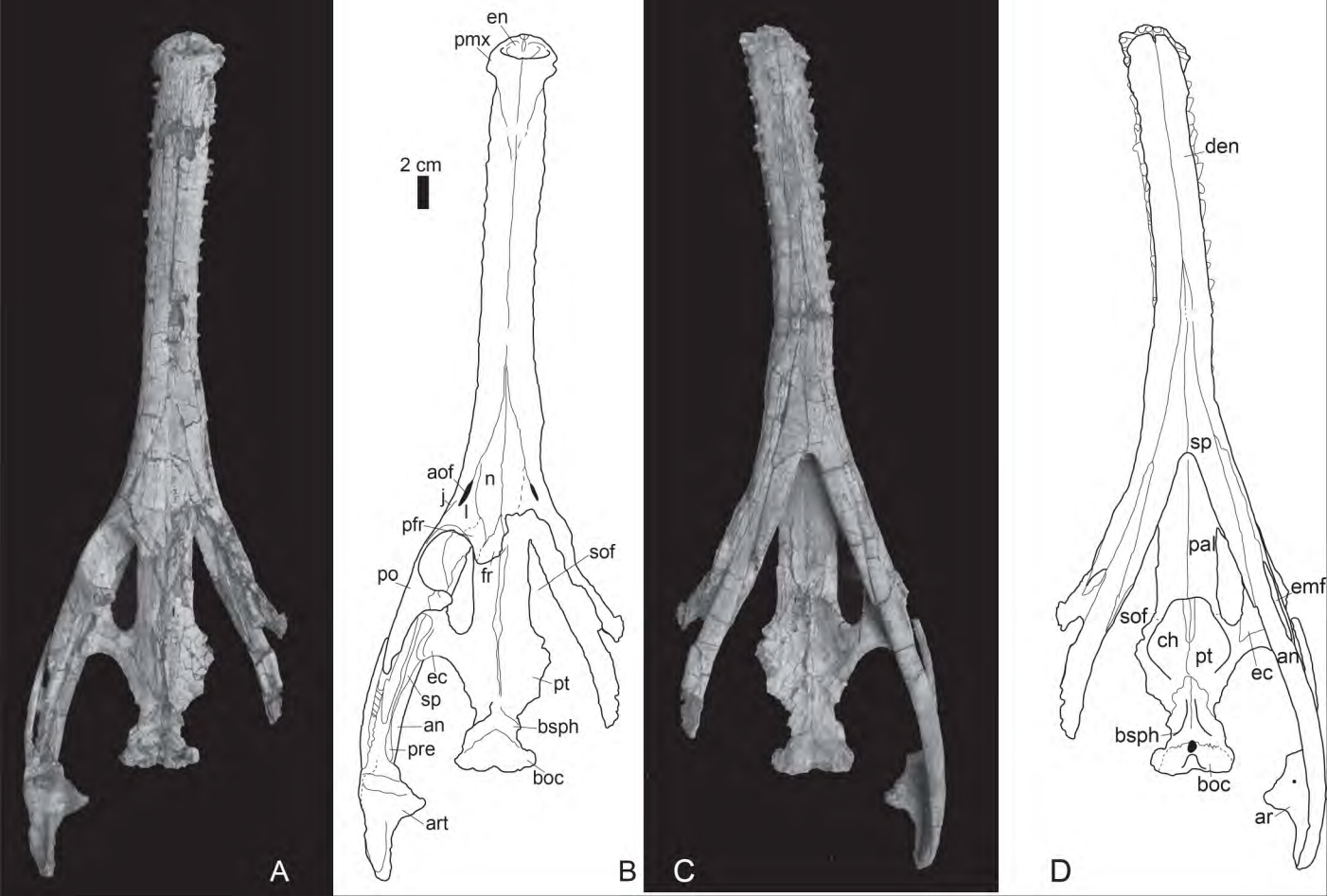
A
en
pmx
2 cm
aof
n
j
l
pfr
sof
po
fr
ec
sp
an
pre
pt
bsph
boc
art
B
C
den
sp
pal
emf
sof
ch
pt
an
ec
bsph
boc
ar
D

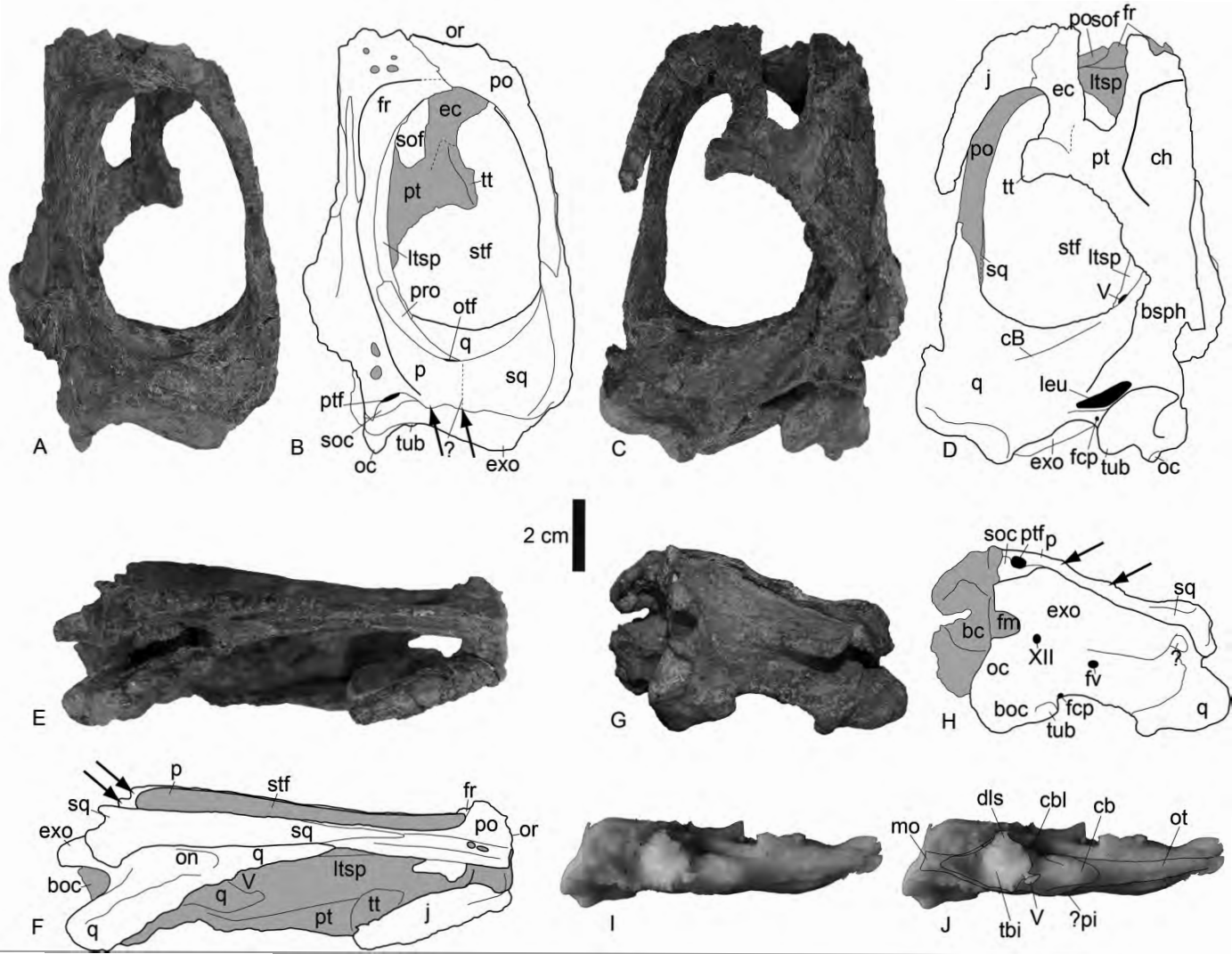
A
B
or
po
fr
ec
sof
tt
pt
ltsp
stf
pro
otf
q
p
sq
ptf
soc
tub
?
exo
oc
C
D
posof
fr
j
ec
ltsp
po
pt
ch
tt
stf
ltsp
sq
V
bsph
cB
q
leu
exo
fcp
tub
oc
2 cm
E
G
H
soc
ptf
p
sq
exo
fm
bc
XII
oc
?
fv
boc
fcp
tub
q
F
p
stf
fr
sq
exo
sq
po
or
on
q
ltsp
boc
q
V
q
pt
tt
j
I
J
dls
cbl
cb
ot
mo
V
tbi
?pi

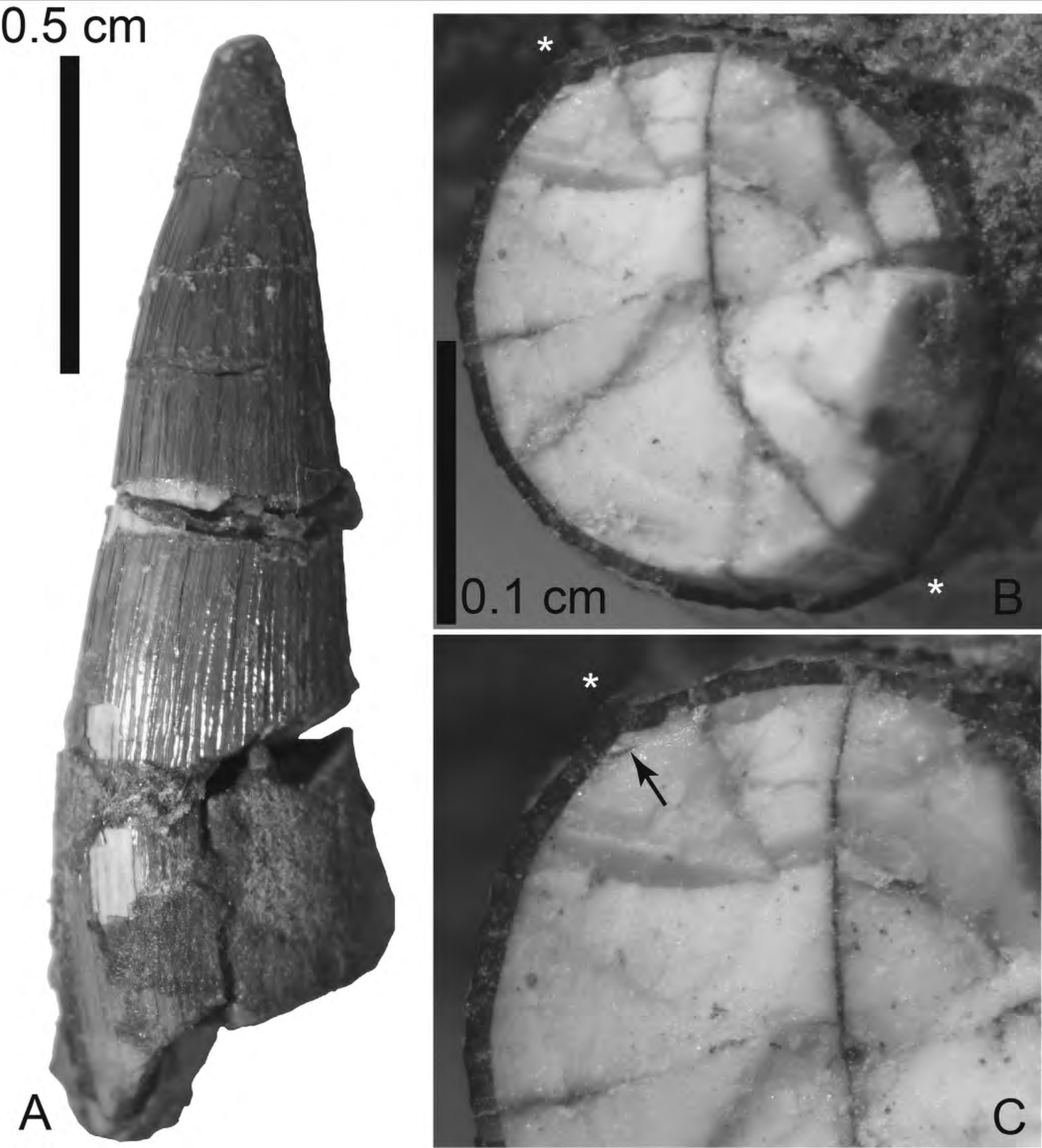
0.5 cm
A
*
0.1 cm
*
B
*
C

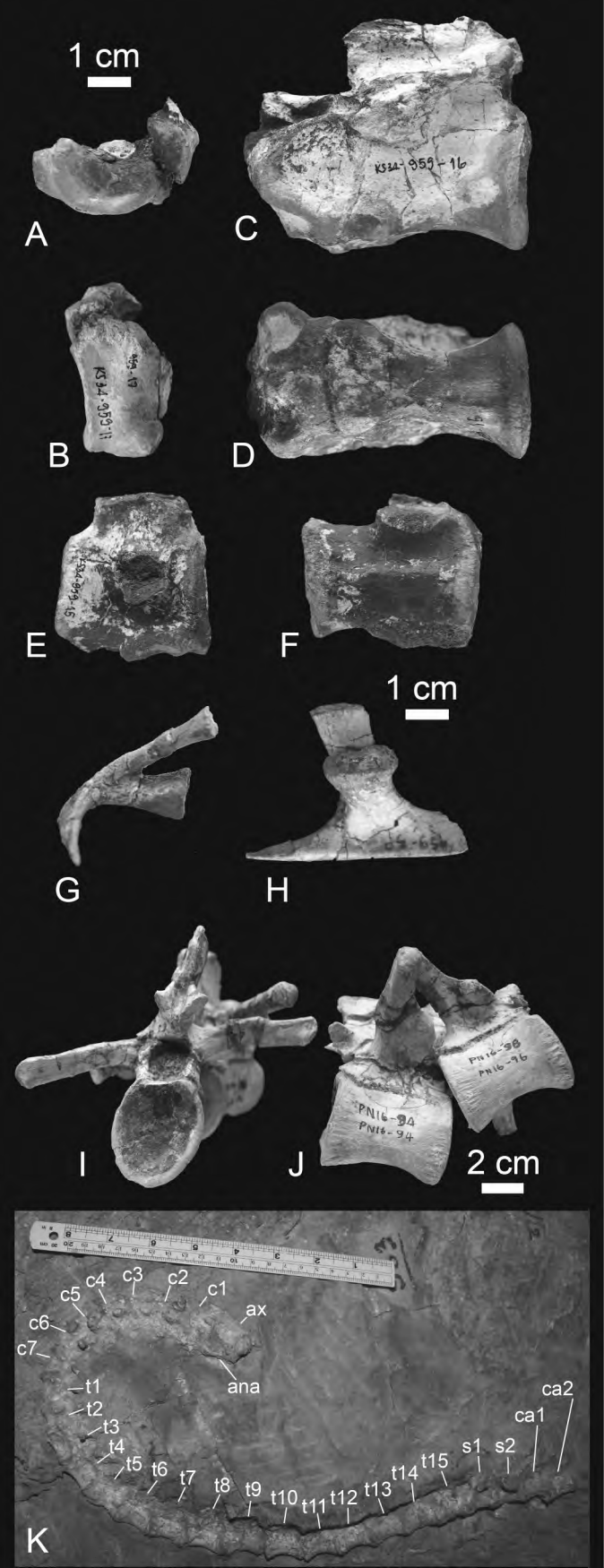
1 cm
A
C
B
D
E
F
1 cm
G
H
I
J
2 cm
c5
c4
c3
c2
c1
ax
c6
c7
ana
t1
t2
t3
t4
t5
t6
t7
t8
t9
t10
t11
t12
t13
t14
t15
s1
s2
ca1
ca2
K

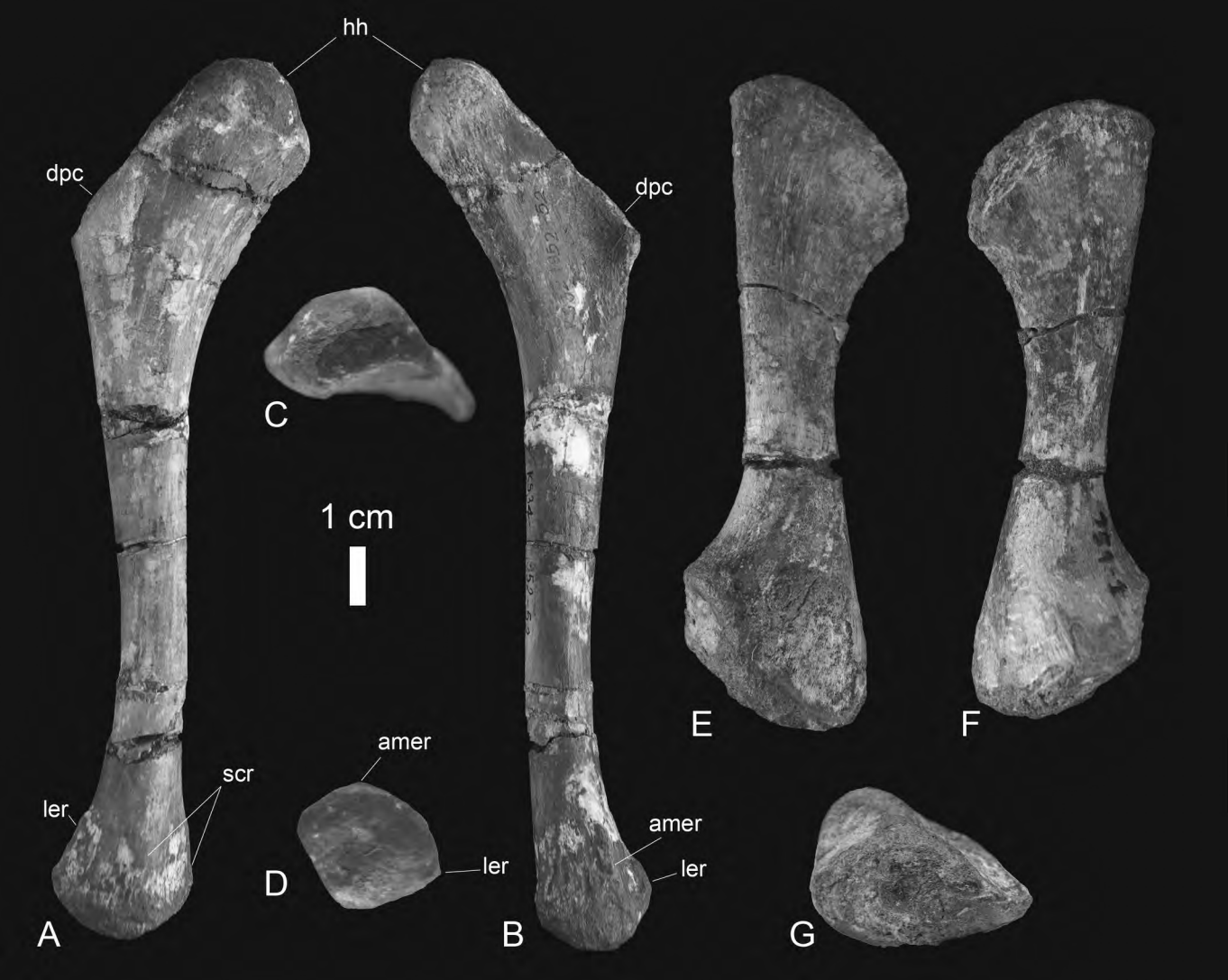
hh
dpc
dpc
C
1 cm
E
F
amer
scr
ler
D
ler
amer
ler
A
B
G


C
peg
4t
ap
E
F
acetf
1 cm
mc
lc
A
B
G
D

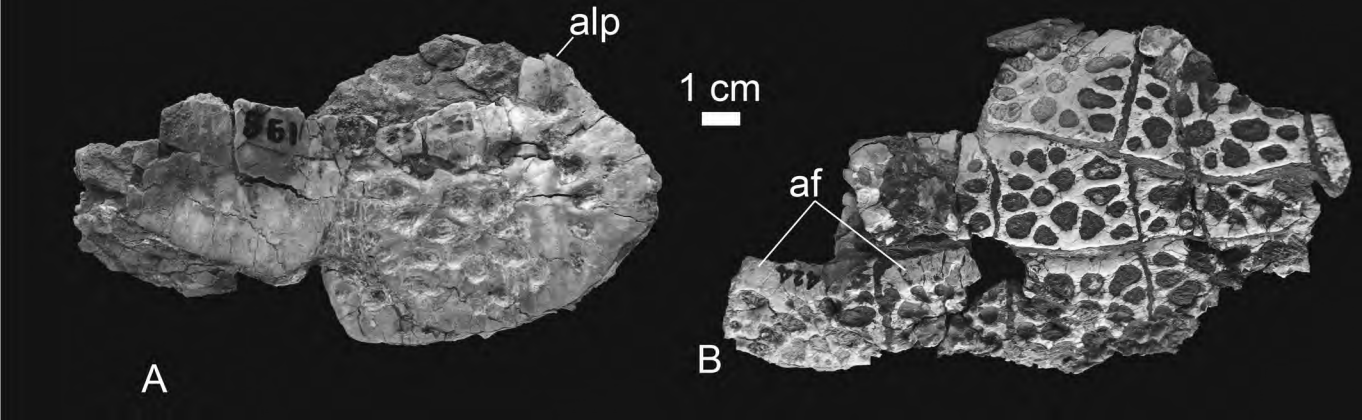
alp
1 cm
af
A
B

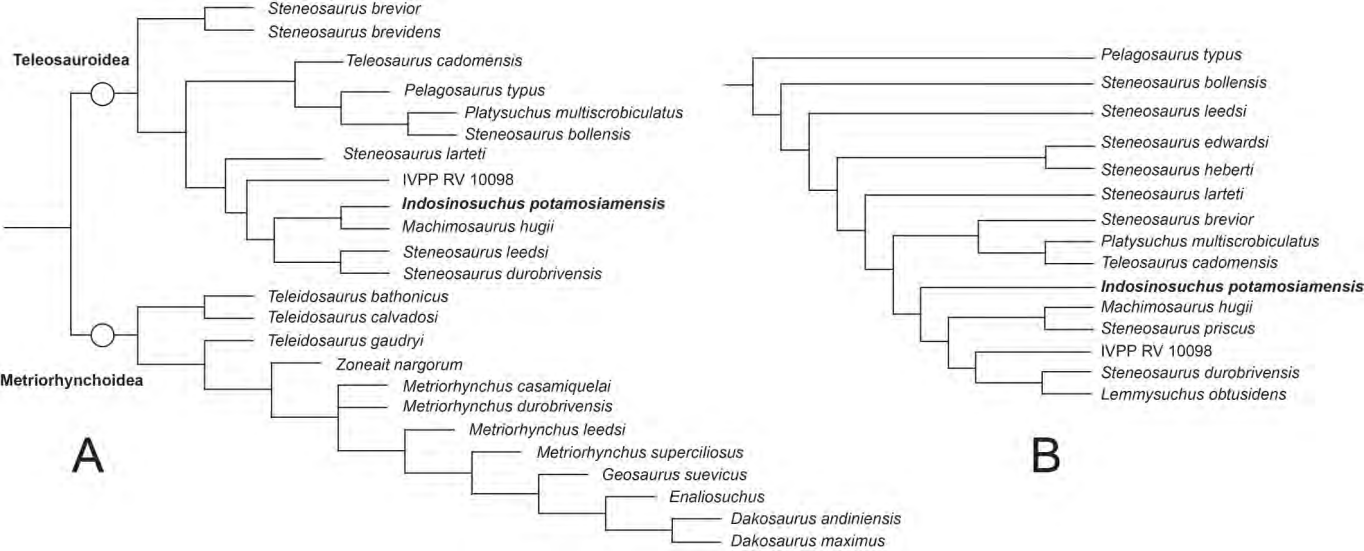
Steneosaurus brevior
Steneosaurus brevidens
Teleosauroidea
Teleosaurus cadomensis
Pelagosaurus typus
Platysuchus multiscrobiculatus
Steneosaurus bollensis
Steneosaurus larteti
IVPP RV 10098
Indosinosuchus potamosiamensis
Machimosaurus hugii
Steneosaurus leedsi
Steneosaurus durobrivensis
Teleidosaurus bathonicus
Teleidosaurus calvadosi
Teleidosaurus gaudryi
Zoneait nargorum
Metriorhynchoidea
Metriorhynchus casamiquelai
Metriorhynchus durobrivensis
Metriorhynchus leedsi
Metriorhynchus superciliosus
Geosaurus suevicus
Enaliosuchus
Dakosaurus andiniensis
Dakosaurus maximus
A
Pelagosaurus typus
Steneosaurus bollensis
Steneosaurus leedsi
Steneosaurus edwardsi
Steneosaurus heberti
Steneosaurus larteti
Steneosaurus brevior
Platysuchus multiscrobiculatus
Teleosaurus cadomensis
Indosinosuchus potamosiamensis
Machimosaurus hugii
Steneosaurus priscus
IVPP RV 10098
Steneosaurus durobrivensis
Lemmysuchus obtusidens
B

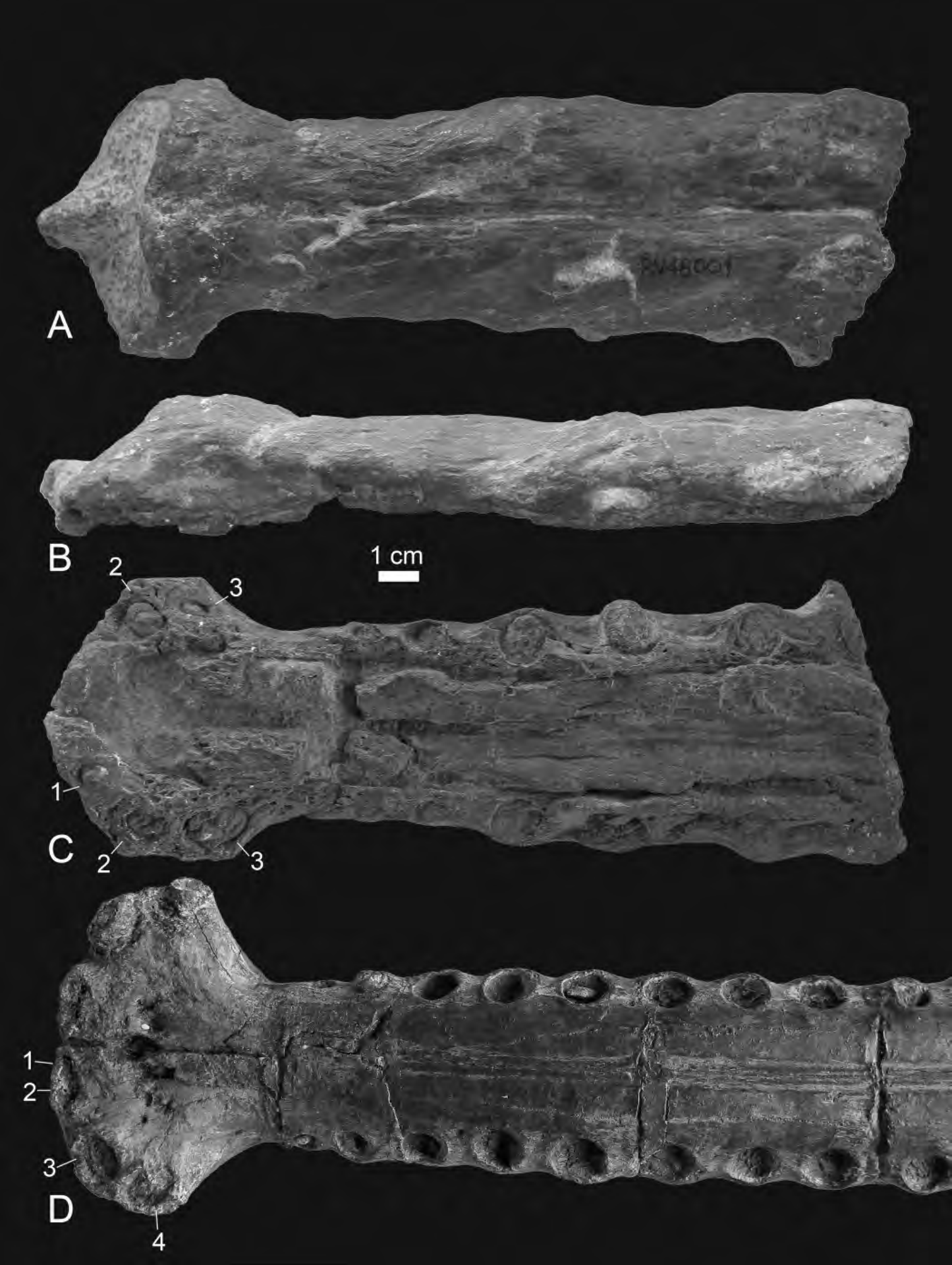
A
B
1 cm
2
3
1
C
2
3
1
2
3
4
D

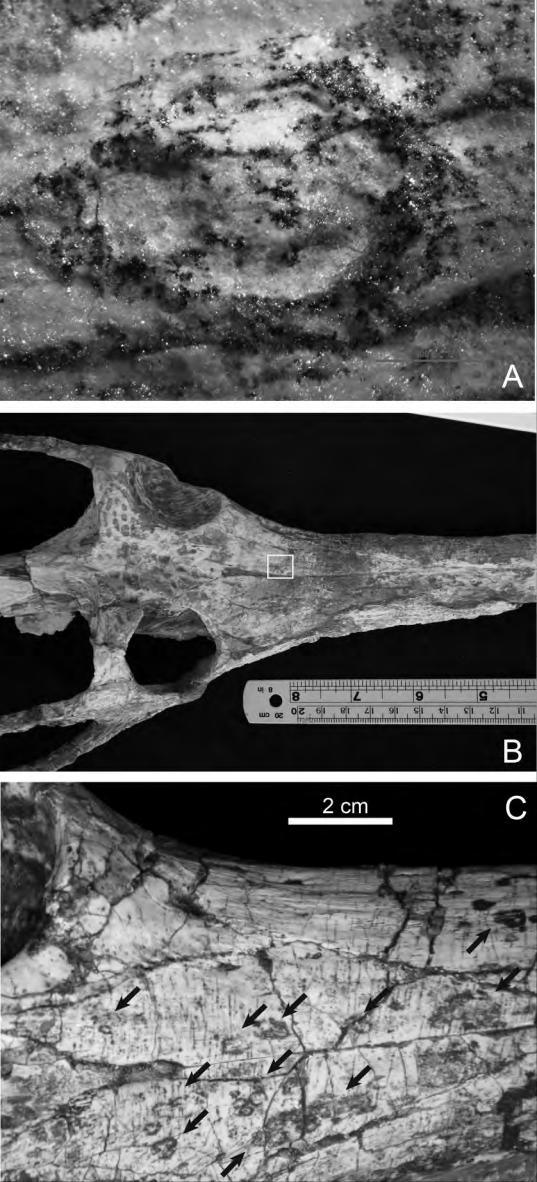
A
B
C
2 cm

APPENDIX 1. Character codings of *Indosinosuchus potamosiamensis* gen. et sp. nov., *Machimosaurus hugii* and IVPP RV 10098 in the data matrix of Wilberg (2015).

Indosinosuchus potamosiamensis

2 1 1 0 1 1 0 2 1 1 0 0
1 0 1 0 2 2 0 1 0 0 1
0 0 1 ? 3 1 0 0 0 2 0
0 0 0 0 0 0 0 2 1 1 1
0 1 1 1 ? ? 0 0 2 1 0
? ? 1 0 0 1 1 1 ? 1 0
0 0 0 1 0 1 0 0 0 0 0
1 0 1 0 1 0 1 0 1 2 0
0 0 0 0 0 1 0 ? 1 0 ?
? ? 0 1 1 2 1 0 0 0 1
2 1 0 1 0 1 0 0 0 ? 1
0 1 1 1 0 1 1 1 1 0 0
0 0 0 ? 1 1 0 1 0 2 1
1 1 0 1 1 3 2 0 ? 1 ?
0 0 0 1 0 1 0 ? 2 3 ?
1 1 ? 0 ? ? 0 1 0 0 0
0 0 1 0 1 0 1 1 0 0 0
0 1 1 1 0 0 ? ? ? ? ?
1 0 ? ? ? ? ? 1 0 1 ?
0 0 0 0 0 0 0 1 1 0 ?
1 0 0 ? ? 0 0 0 1 1 1

APPENDIX 1. (Continued)

1	0	0	0	0	1	1	0	1	?	1	2
	0	0	0	0	0	1	0	0	?	0	0
	0	1	0	0	1	1	0	0	0	0	0
	0	1	0	0	1	0	0	1	0	?	1
	0	0	1	?	0	0	1	1	?	0	0
	0	1	0	0	?	0	?	?	?	0	0
	1	0	0	0	1	0	0	1	0	0	0
	0	0	?	0	1	0	1	1	?	?	0
	?	0	0	0	?	0	0	0	1	0	1
	0	1	0	0	0	0	1	0	0	?	0
	0	0	0	1	?	0	0	0	?	2	0
	?	1	0	0	1	0	1	?	1	0	0
	0	0	0	?	0	?	?	0	0	0	

Machimosaurus hugii

2	1	1	0	1	1	0	3	1	1	0	0
	1	0	1	0	2	0	0	1	0	0	1
	1	0	1	?	3	1	0	?	0	2	0
	0	1	0	0	0	0	2	2	1	?	1
	?	1	?	?	?	?	?	0	?	1	0
	?	?	1	0	0	1	1	0	?	1	0
	?	0	0	1	0	1	0	0	0	0	1
	1	0	1	0	1	0	1	0	1	2	0
	0	0	0	0	0	1	0	?	1	0	?

APPENDIX 1. (Continued)

?	?	0	2	1	2	1	0	0	0	1
2	1	0	1	0	?	0	0	0	?	1
0	1	1	1	0	1	?	1	1	0	0
0	0	0	?	1	1	?	1	0	1	1
1	1	0	1	1	3	2	0	1	1	0
0	0	0	1	0	1	0	0	2	3	?
1	1	?	0	0	?	0	2	0	1	0
0	0	1	0	1	0	0	1	1	0	0
0	1	1	1	?	?	?	2	1	?	?
?	?	?	?	?	?	?	?	?	?	?
0	?	0	0	0	?	?	1	?	0	?
?	?	?	?	?	0	0	0	1	1	1
1	0	0	?	0	1	?	0	0	?	?
?	0	0	0	0	0	1	0	0	?	0
0	0	1	0	0	0	1	0	0	0	0
0	0	1	0	0	1	0	0	1	0	?
?	0	0	1	?	0	0	1	0	0	0
0	?	?	0	1	?	?	?	?	?	0
0	1	0	0	?	?	0	0	?	0	0
0	0	0	?	0	1	0	1	?	?	?
0	?	0	0	0	?	0	0	0	?	1
1	0	1	0	0	0	0	0	0	0	?
0	0	0	0	?	?	0	0	0	?	2

APPENDIX 1. (Continued)

	0	?	?	0	0	1	?	?	0	1	?
	0	0	0	0	?	0	?	?	0	0	0

IVPP RV 10098

2	1	1	0	1	1	0	2	1	1	0	0
	1	0	1	0	2	2	?	1	0	0	1
	?	0	1	?	3	1	0	?	1	2	0
	0	0	0	0	0	0	0	2	1	?	1
	0	1	1	?	?	?	?	0	2	1	0
	?	?	?	?	?	?	1	1	?	?	0
	0	0	0	?	?	?	?	?	?	?	0
	1	0	1	0	1	0	1	?	1	2	0
	0	0	1	0	0	1	0	?	0	0	?
	?	?	0	1	1	2	1	0	0	0	0
	?	1	0	1	0	1	0	?	0	1	1
	?	?	?	?	?	?	1	1	?	0	0
	?	0	0	1	1	?	?	0	0	1	1
	0	1	0	1	1	?	?	?	?	?	?
	?	?	?	?	?	?	?	?	?	?	?
	?	?	?	?	?	?	0	1	0	0	0
	0	0	1	0	1	0	1	1	1	0	0
	0	?	?	1	?	?	?	?	?	?	?
	?	?	?	?	?	?	?	?	?	?	?
	?	?	?	?	?	?	?	?	?	?	?

APPENDIX 1. (Continued)

?	?	?	?	?	0	0	0	1	?	1
?	0	0	0	?	?	?	0	1	1	1
2	0	0	0	0	0	1	1	?	?	?
?	?	1	0	?	0	1	?	0	0	?
0	?	1	0	0	?	?	0	1	0	?
1	0	0	1	0	?	?	?	?	?	?
?	?	?	?	?	?	?	?	?	?	?
0	1	0	0	0	1	0	0	1	?	0
0	0	?	0	0	0	0	?	?	?	?
0	?	0	?	?	?	0	0	0	1	1
0	?	1	0	0	0	0	0	0	0	?
?	?	?	?	?	?	?	0	?	?	0
?	?	?	?	?	?	?	?	0	?	?
0	0	?	0	?	0	?	?	0	0	?

APPENDIX 2. List of characters used in the small datamatrix for exploring interrelationships of teleosaurids.

Ch. 1: dimensions of orbits relative to interorbital width: nearly equal/larger (0) or much smaller (1).

Ch. 2: antorbital fenestra: small but present (0) or absent (1).

Ch. 3: nasal length: as long or longer than length of supratemporal fenestrae (0) or shorter (1).

Ch. 4: maxillary alveolar count: over 30 (0) or less than 30 (1).

Ch. 5: anterior margin of supratemporal fenestra: gently convex (0) or perpendicular to sagittal plane (1) or pointed (2).

Ch. 6: supratemporal fenestra length/width ratio: equal or no more than 1.5 (0) or markedly longer than wide with ratio at or over 1.8 (1).

Ch. 7: antorbital over total skull length ratio: mesorostrine, i.e. < 0.7 (0) or longirostrine, i.e. ratio between 0.75 and 1.00 (1).

Ch. 8: premaxillae in line with lateral edges of maxillary rostrum (0) or laterally expanded (1) in dorsal view.

Ch. 9: premaxillary alveolar count: three (0) or four (1).

Ch. 10: posterior processes of nasal stop near mid-length level of prefrontal (0) or nearly reach posterior level of prefrontal (1).

Ch. 11: surface of tooth enamel ornamented with vertical ridges (0) or with discontinuous wrinkles.

Ch. 12: orbits facing laterally (0) or mostly dorsally (1).

APPENDIX 2. (Continued)

Ch. 13: in dorsal view, parietal exposure on posteromedian margin of skull table: restricted to posteriormost portion (0) or extends as a limited surface between the supratemporal fenestrae (1).

Ch. 14: humerus versus femur length: about one third shorter than femur (0) or less than half the length of femur (1).

Ch. 15: sacral vertebrae count: two (0) or three (1)

Ch. 16: dorsal shield comprises subrectangular osteoderms (0) or also includes elements wider than long (1) in the posterior half of the trunk.

Ch. 17: anterior half of external mandibular fenestra narrower (0) or of same height (1) as posterior half.

Ch. 18: lateral margin of skull table as wide as orbital margin of skull (0) or wider (1).

APPENDIX 3. Datamatrix used in this work for exploring the intrarelationships of teleosaurids.

P_typus		0	0	0	1	0	0	1	0	1
0	0	0	0	0	0	0	0	0		
T_cadomensis		0	0	0	0	2	0	1	1	1
1	?	1	1	1	?	1	1	1		
P_multiscrobiculatus		0	0	0	0	2	0	1	1	
0	0	0	1	1	0	0	1	0	1	
S_bollensis		0	0	0	1	1	0	1	0	[0,1]
1	0	1	0	0	0	0	0	0		
S_leedsi		0	0	1	0	0	1	1	0	1
1	0	1	0	?	0	1	?	0		
L_obtusidens		0	0	1	1	0	1	0	1	1
0	1	1	0	?	1	1	?	0		
S_priscuscanjuers		1	1	0	?	1	1	1	1	
1	0	0	1	?	1	1	?	?	?	
*Machimosaurus*_sp		1	1	?	1	1	1	0	1	
0	0	1	1	1	?	1	1	1	0	
S_durobrivensis		0	0	1	1	0	1	0	1	
1	0	1	1	0	1	0	1	?	0	
IVPP RV 10098		0	0	1	1	1	1	0	1	
1	0	0	1	0	?	?	?	?	0	
S_brevior		0	0	0	?	1	0	0	1	0
0	0	1	1	?	?	?	0	0		

APPENDIX 3. (Continued)

Indosinosuchus			0	0	0	1	1	1	0	1
1	1	0	1	1	0	0	1	1	0	
S_heberti		0	1	1	0	0	1	0	1	0
0	0	1	0	?	?	?	0	1		
S_edwardsi		0	1	0	1	0	?	0	0	?
1	?	1	?	?	?	?	?	1		
S_larteti		0	0	0	0	0	1	0	0	1
0	?	1	1	?	?	?	?	0		